Biosensors and Bioelectronics 85 (2016) 536–552

Contents lists available at ScienceDirect

Biosensors and Bioelectronics

journal homepage: www.elsevier.com/locate/bios

Carbon nanotube modification of microbial fuel cell electrodes

Alireza Ahmadian Yazdi [a], Lorenzo D'Angelo [a], Nada Omer [a], Gracia Windiasti [b], Xiaonan Lu [b], Jie Xu [a,*]

[a] Department of Mechanical and Industrial Engineering, University of Illinois at Chicago, Chicago, IL, USA
[b] Faculty of Land and Food Systems, The University of British Columbia, Vancouver, British Columbia, Canada

ARTICLE INFO

Article history:
Received 23 February 2016
Received in revised form
21 April 2016
Accepted 8 May 2016
Available online 10 May 2016

Keywords:
Carbon nanotube
Microbial fuel cell design
Nanocomposites
Oxygen reduction reaction
Thin film fabrication

ABSTRACT

The use of carbon nanotubes (CNTs) for energy harvesting devices is preferable due to their unique mechanical, thermal, and electrical properties. On the other hand, microbial fuel cells (MFCs) are promising devices to recover carbon–neutral energy from the organic matters, and have been hindered with major setbacks towards commercialization. Nanoengineered CNT–based materials show remarkable electrochemical properties, and therefore have provided routes towards highly effective modification of MFC compartments to ultimately reach the theoretical limits of biomass energy recovery, low–cost power production, and thus the commercialization of MFCs. Moreover, these CNT–based composites offer significant flexibility in the design of MFCs that enable their use for a broad spectrum of applications ranging from scaled–up power generation to medically related devices. This article reviews the recent advances in the modification of MFCs using CNTs and CNT–based composites, and the extent to which each modification route impacts MFC power and current generation.

Contents

* Corresponding author.
E-mail address: jiexu@uic.edu (J. Xu).

http://dx.doi.org/10.1016/j.bios.2016.05.033
0956-5663/

1. Introduction

Since the discovery of carbon nanotubes (CNTs) in1991 by Ijiima and colleagues (Iijima, 1991), CNTs have drawn a great deal of attention due to their unique features. CNTs are lengthy (up to millimeters), narrowed (1–100 nm) cylindrical structures of carbon atoms that are often capped at each end (Hoenlein et al., 2004; Thostenson et al., 2001). These tubular structures, often classified as SWCNT (single–walled or single tube) and MWCNT (multi–walled or concentric tubes), possess individually unique mechanical properties such as extremely high elastic modulus [higher than 1 TPa (Treacy et al., 1996)] and tensile strength [up to 63 GPa (Yu et al., 2000)], as well as excellent thermal (Berber et al., 2000) and electrical conductivity [92 Scm^{-1} (Bradford and Bogdanovich, 2008)]. Highly purified CNTs are extensively used as building blocks of advanced materials with remarkable properties. Owing to the attractive features of pristine CNTs including lightweight, high surface area to volume (SAV) ratio, adsorption properties, biocompatibility, and magnetic properties, CNT–based structures find their use in a wide collection of applications, including microelectronics (Bottacchi et al., 2015; Franklin et al., 2012; Held et al., 2015), tissue engineering (Bosi et al., 2014; Hopley et al., 2014), biosensors (Esser et al., 2012; Kurkina et al., 2011; Rivera et al., 2015; Shi et al., 2011; Zhao et al., 2012), energy–storage materials (Chen et al., 2014; Yu et al., 2014), and biological delivery systems (Al Faraj et al., 2015; Cai et al., 2005; Kam et al., 2005).

Electrical energy can be produced by microorganisms that are capable of exocellular electron transfer, often referred to as "exoelectrogen" (Logan, 2009). Microbial fuel cells (MFCs) generate electricity by utilizing these exoelectrogens as biocatalyst to oxidize organic matters, such as glucose, acetate, and lactate (Fig. 1). The bacterial respiration or metabolic activity breaks down the organic matter (electron donor) into electrons, protons, and carbon dioxide. Afterwards, the liberated electrons are exocellularly transported to a conductive surface (anode), and travel through an external circuit to produce power. Eventually, electrons are collected at a positive terminal (cathode) where they are combined with the protons, that have already travelled inside the electrolyte from the anode to the cathode by probably passing through a membrane, and oxygen (electron acceptor) to form water. Due to their flexibility in exploiting diverse sources of bacteria, MFCs find applications in energy recovery from biomass (Baranitharan et al., 2015; Hernández-Fernández et al., 2015; Liu et al., 2004; Logan et al., 2015; Tee et al., 2016), miniaturized power supplies (Choi, 2015; Mink et al., 2014; Ren et al., 2014; Vigolo et al., 2014), biosensors and biofilm studies (Jayasinghe et al., 2014; Jiang et al., 2015; Katuri et al., 2012; Lu et al., 2015; Malvankar et al., 2012; Rasmussen and Minteer, 2015), hydrogen production (Carmona-Martínez et al., 2015; Catal et al., 2015; Kuntke et al., 2014; Logan et al., 2008; Zhang and Angelidaki, 2014), and chemical synthesis systems (Li, 2016; Müller 2016; Sakimoto et al., 2016).

CNTs and CNT–based composites have been used as components of MFCs since a decade ago. These emerging nanoengineered

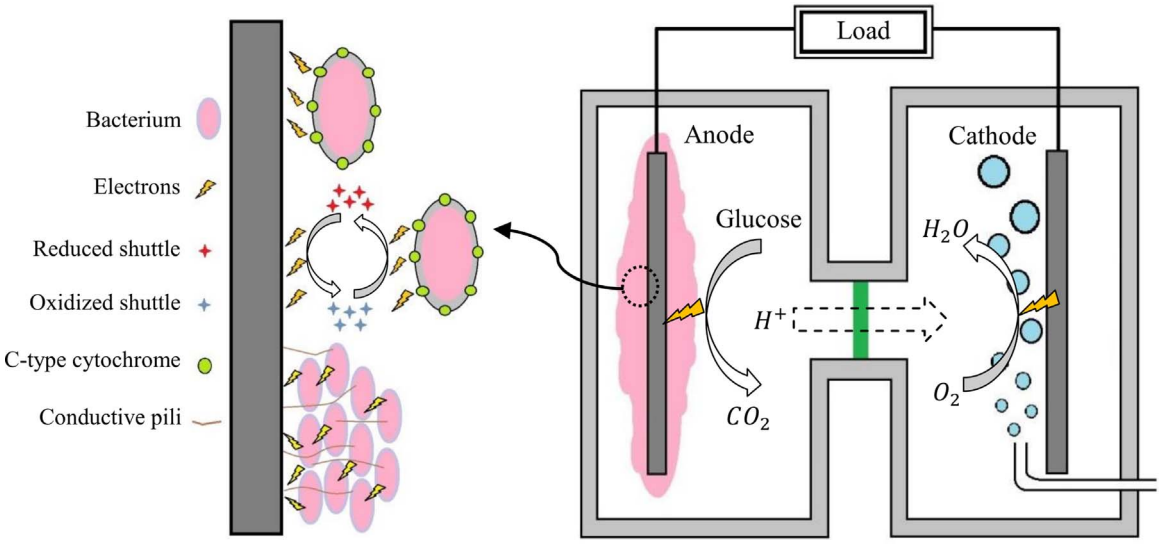

Fig. 1. (Right) Operating principle of a conventional MFC; the bacterial community known as biofilm (pink) which has colonized the anode surface catalyzes the oxidation of organic matters, releases carbon dioxide and protons, and transports the electrons to the anode. At the cathode, oxygen (mainly) is reduced with the help of metallic catalysts (in conventional MFCs) to form water, as shown in the figure. Often a membrane (green) is utilized to enhance the filtration of protons between the anode and cathode chambers, whereas in laminar–flow MFCs (Li et al., 2011) this membrane is removed due to the relatively high molecular diffusion of cations compared to low convective mixing of co–flowing streams at micro scale. (Left) Extracellular electron transfer (EET); in a multilayer biofilm, layers close to the anode surface transfer electrons via direct contact or electron shuttles (mediators), while for outer layers the electrons are mainly transported via bacteria self–produced conductive pili known as nanowires. The left image is adapted with permission from Kumar et al. (2015), Copyright © 2015. (For interpretation of the references to color in this figure legend, the reader is referred to the web version of this article.)

materials aim to improve MFC in two aspects: electrochemical activities of the bacterial community at the anode, and oxygen reduction reaction (ORR) at the cathode. Note that, in this categorization we exclude the use of biocathodes where bacterial communities or enzymes act as electron acceptor (Wang et al., 2013b; Xia et al., 2013). Recently, Ci et al. (2015) have reviewed the performance improvement of MFC by exploiting graphene–based materials with major emphasis on two–dimensional graphene sheets as either catalyst or support material for electrodes. Moreover, Antolini and coauthors (Antolini, 2015) presented an overview of the MFC application of composite materials, including metal/polymer, metal/carbon, and polymer/carbon composites, whereas in another article the electrode materials were reviewed in a more inclusive approach (Mustakeem, 2015). While acknowledging their tremendous efforts, a review which addresses the CNTs incorporation into the MFCs would be beneficial to both MFC research community and nanomaterial researchers, due to the ever–increasing demand for novel CNT–based materials in bioenergy harvesting devices. In this regard, the present article aims to highlight the most recent advances in exploiting CNTs and CNT composites in MFCs by providing a review of the fast, facile, and low–cost techniques for the preparation of CNT modified electrodes. We first begin by understanding the synthesis process of CNTs, functionalized CNTs, and the preparation methods of CNT–based MFC electrodes. Then, the effect of newly synthesized composites on MFC performance are discussed according to recent reports, followed by discussing the challenges and opportunities on the scaling–up and commercialization of the MFC with the aid of CNTs.

2. Towards the fabrication of CNT–based electrodes

2.1. Synthesis of pristine CNTs

Individual CNTs can be mass–produced by three commonly used method, namely, arc–discharge (Journet et al., 1997), laser ablation (Thess et al., 1996b) and chemical vapor deposition (CVD) (Cassell et al., 1999). Arch discharge and laser ablation produce high quality CNTs by evaporating a solid carbon source, and subsequent condensation in an inert gas, such as argon or helium (Fig. 2). In arc discharge, the energy of a high–temperature plasma discharged between two graphite electrodes is used for the evaporation of carbon source, whereas in laser ablation this high temperature is provided by laser energy (Journet et al., 1997; Thess et al., 1996a). In contrast to CVD, laser ablation and arc discharge are faced with major setbacks for being used as a cost–effective manufacturing technique mainly due to the high temperature ($\geq$3000 °C) of the reaction environment limiting the quantity of CNTs that these methods can synthesize (Cassell et al., 1999). In CVD, however, bulk amounts of high quality CNTs can be yielded via reaction between the gaseous hydrocarbon feedstock and transition metal catalyst particles, as shown in Fig. 2 (Baker, 1989).

2.2. Functionalization of CNTs

As-prepared CNTs may vary in diameter, length, and structure, and more importantly are often conjugated with impurities of carbonaceous byproducts and/or metal residues that hamper their unique properties. Thus, various functionalization routes are required to remove the impurities and pave the way for synthesis of other CNT–based hybrid materials suitable for a desired application. CNT functionalization can be achieved mainly via covalent attachment of functional groups through a chemical reaction, or adsorption or wrapping the CNTs with different groups like polymers, biomolecules, and metal nanoparticles (Karousis et al., 2010).

In principle, preformed metal nanoparticles (NPs) can be connected to the CNT structure via covalent linkage or weaker bonds (indirect approach), or being grown and/or deposited onto the CNT structure (direct procedure) (Georgakilas et al., 2007; Karousis et al., 2010). In the direct procedure, the adhesion of metal NP with van der Waals interaction occurs via a reduction process in the presence of CNTs in which noble metals are used as the precursor. This process can be assisted by heat, light, and reducing agents (Georgakilas et al., 2007). Metal NPs interaction with CNTs via covalent linkage can be achieved via functional groups present on NPs for efficient connection to the CNTs, known as linkers (Dubal et al., 2013). These linkers may lead to the formation of covalent bonds with the functional groups present on the CNT surface, or bond with weak intermolecular interaction namely π – stacking, hydrophobic, and electrostatic interactions. CNTs may also be functionalized with polymer functional groups that are physically adsorbed onto the CNT surface, or covalently bonded to its structure. The commonly used process of polymer functionalization of CNTs is the solution casting techniques, where CNTs and polymers are mixed in a solvent, followed by evaporation of the solvent to obtain the polymer/CNT composite (Byrne and Gun'ko, 2010; Lee et al., 2010). However, these conventional techniques as well as low–tech methods of casting or dip–coating for the fabrication of conductive cross–linked polymer matrix, exhibit low control over the finished composite and material waste. New approaches include the class of layer–by–layer (LbL) assembly techniques that have been extensively used for the synthesis of highly functional electrodes for batteries and fuel cells (Hyder et al., 2011; Lee et al., 2008; Paloniemi et al., 2006). Many variations of LbL have been proposed among which spin–spray layer–by–layer (SSLbL) introduced by Merrill et al. (Merrill and Sun, 2009) is notable. Their synthesis method later upgraded by Gittleson et al. (2012) to be an automated and highly fast assembly of polyelectrolyte/CNT films within 13 s, with the possibility of reducing the cycle times to even subseconds. Other features include reduction in costly material

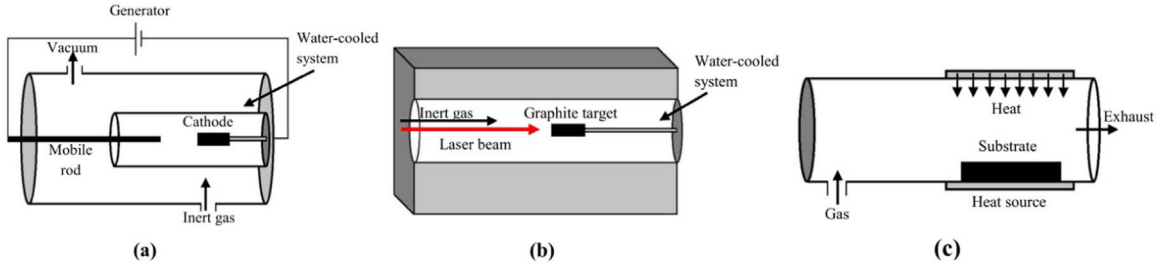

Fig. 2. In arc discharge, the energy of a high–temperature plasma discharged between two graphite electrodes evaporates the graphite, which then rapidly condenses to grow CNTs. (b) Laser ablation, however, takes advantage of a high temperature laser energy to sublime a carbon source followed by condensation of carbon vapor within a flow of helium or argon. (c) In CVD a gaseous hydrocarbon is fed into the furnace where it is cracked into carbon and hydrogen, and finally precipitates as CNTs onto the catalyst bed. Adapted from Journet and Bernier, (1998), Copyright © 1998, with permission from Springer.

waste, homogenization of thin film conductance, and nanolevel control over the film growth.

2.3. Assembly of CNT–based materials

CNTs have been synthesized into many macroscopic structures namely aerogels, sponges, foams, arrays, wafers, yarns, and sheets. Each of these structures offers unique features, physical parameters, and functionalities that vary greatly from those of as-prepared or functionalized CNTs. For many applications including electrodes of energy storage/conversion devices, CNTs and CNT composites are assembled either as 2D thin films supported by a conductive substrate, or 3D monolith/free-standing structures.

2.3.1. CNT–based thin films

CNT thin films can be directly grown on a substrate such as silicon oxide in a CVD furnace at a temperature often between 500 and 1200 °C (Souza et al., 2015), and further modified with functional groups. This technique enables control over the surface features of the CNT network in terms of alignment, porosity, and density, with the help of catalyst nanoparticles, surface features of the substrate, and CVD parameters. In a simpler manner, as–prepared CNTs can be coated or deposited onto a desired substrate at room temperature to produce a conductive thin film for use as electrode (Ghasemi et al., 2013). This technique involves a multi–step wet–chemistry process that is often comprised of acid treatment of pristine CNTs, followed by dispersion in an organic solvent often with the aid of surfactants. Compared to the direct growth of CNTs on a substrate this technique can be scaled–up to commercial levels; however, it uses harsh chemicals and surfactants that negatively influence the electrical conductivity of the CNT networks, if they remain in the deposited thin film.

Many autoclavable and chemically resistant polymers (e.g., polycarbonate and acrylic glass) are quite popular for laboratory design and fabrication of MFCs. However, they may not be directly used in some of the CNT film fabrication techniques mentioned so far, as they cannot undergo high temperature of CVD furnace or cannot be used as a substrate for depositing the CNT solution containing surfactants. These issues along with the need for patterning the CNT network on the polymer substrate in accordance with the MFC design requirements, necessitate the use of printing methods of CNT thin films onto a receiving substrate that are briefly covered in Fig. 3. From a general standpoint, CNT thin film transfer can be divided as either a wet or dry process. Often these techniques are assisted by heat, pressure, laser, etc., in the pursuit of removing the surfactants, and improving the process speed and quality of the transferred pattern. Dry transfer of CNTs is often governed by the interfacial binding energy of the substrates involved in the transfer; the sacrificial substrate or the substrate transporting the CNTs should possess lower surface energy than both target and initial substrates. Due to the lower surface energy compared to many polymers used in MFC design and fabrication, PDMS is a popular material for fast and facile film transfer between the initial and target substrate which can also undergo soft

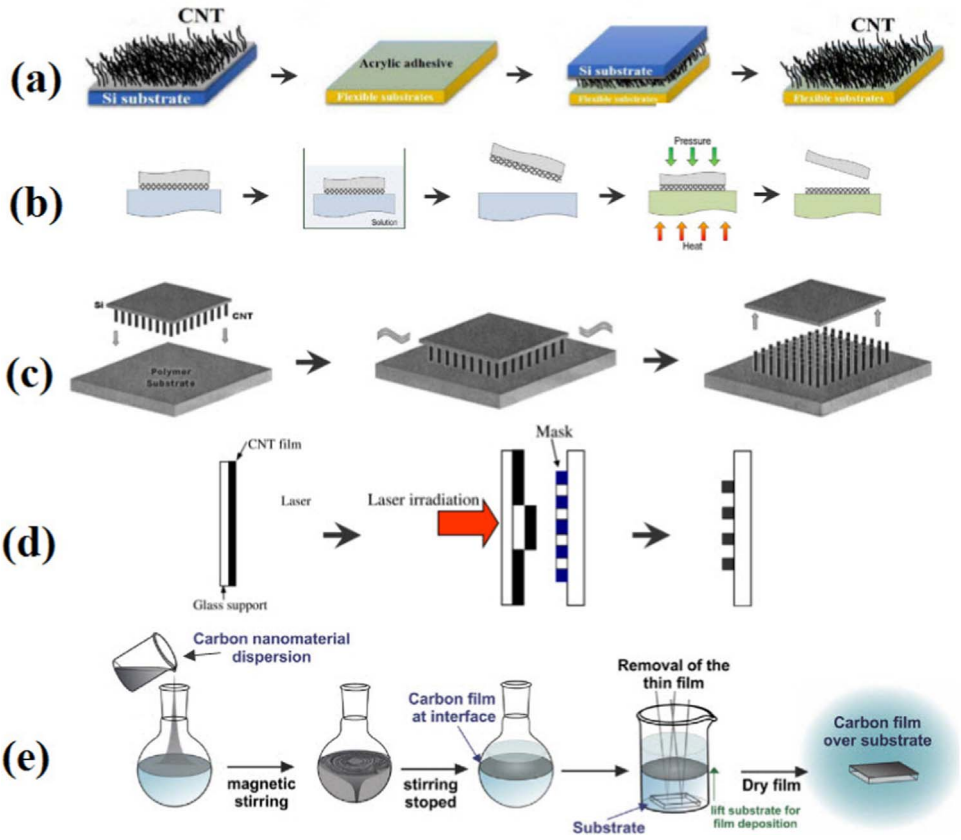

Fig. 3. (a) Adhesive transfer of CNTs grown on silicon substrate with the aid of acrylic adhesive. Adapted with permission from Lin et al. (2015). (b) Transfer printing; the PDMS stamp acquires the CNT film sprayed on a glass substrate followed by immersing in water. PDMS is then peeled off and transports the pattern to a desired substrate via heat and pressure assistance. Reprinted from Abdelhalim et al. (2013), Copyright 2013, with permission from Elsevier. (c) Microwave assisted transfer; a polymer transporter is loaded with CNT forest grown on silicon substrate. The loading process is assisted by heating the CNTs via microwave. Reprinted with permission from Sunden et al. (2006), Copyright 2006, American Vacuum Society. (d) Laser assisted transfer; the CNT thin film on the initial substrate undergoes a sequence of evaporation enabled by laser pulse energy and deposition on the patterned substrate. Adapted with permission from Chang-Jian et al. (2006). (e) Liquid–liquid interface transfer; the mixture of CNT with an organic solvent and an aqueous solution is stirred well, and then kept at rest until a film is formed at the liquid–liquid interface. Eventually a substrate within the mixture is pulled out in a bottom to top direction to have the thin films adhered to the surface. Reprinted from Souza et al. (2015), Copyright 2015, with permission from Elsevier.

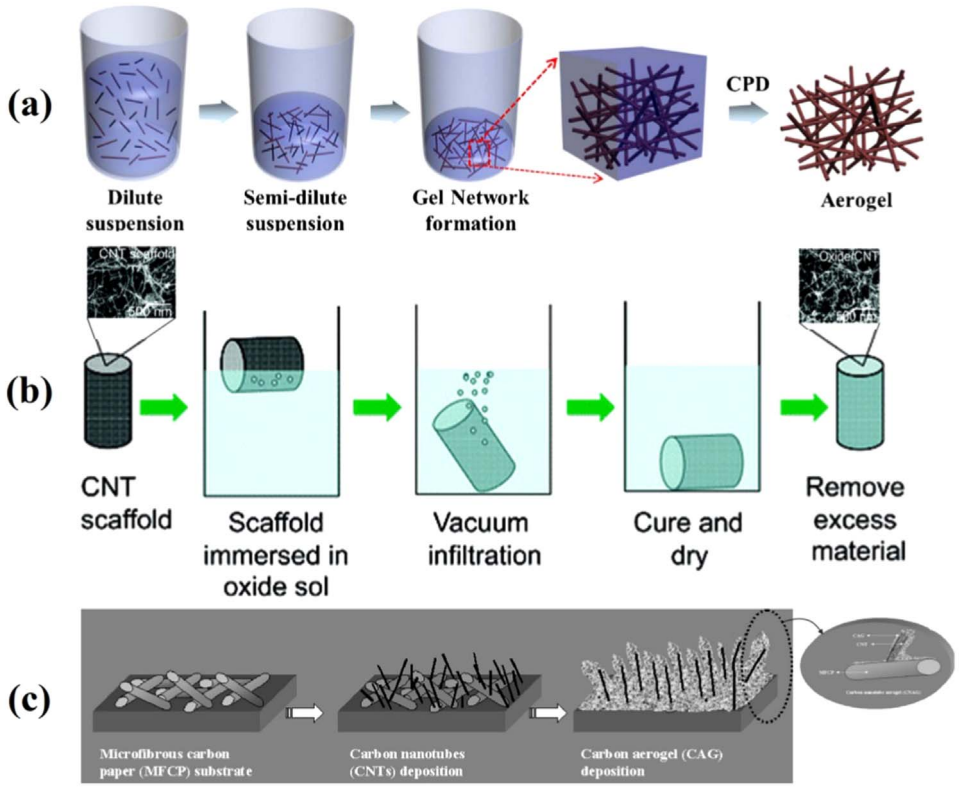

Fig. 4. Schematic illustration of the CNT–based aerogel synthesis process: (a) A novel synthesis composed of preparing the CNT containing suspension, increasing the concentration of colloids until the gel is formed, and eventually extracting the solvent by supercritical drying. Reprinted by permission from Macmillan Publishers Ltd.: Scientific Reports (Jung et al. 2012), Copyright 2012. (b) Synthesis of composite aerogels of metal oxide/CNTs via a sol–gel process. Reprinted with permission from Worsley et al. (2011) American Chemical Society, Copyright 2011. (c) Synthesis of aerogel on the CNTs grown on a microfibrous carbon paper. Reprinted with permission from Bordjiba et al. (2008), Copyright 2008.

lithography to transfer a pattern of CNT network as dictated by the configuration of MFC compartments. A more difficult and delicate approach is the wet transferring of thin films by using many commercially available CNT solutions. This method is often accompanied by subsequent thermal annealing process to remove the surfactants from the solution.

2.3.2. CNT–based monolith structures

In recent years, 3D monolith structures have gained profound interest, as they fully expose CNTs surface for catalysis and adsorption of chemical groups, while offering high electrical conductivity as a free–standing electrode. Many variations of these 3D structures have been developed based on CNTs, while here we turn our attention to the synthesis of three classes of them namely aerogels (Nardecchia et al., 2013), foams (Bradford et al., 2011), and sponges (Cheng et al., 2015), which are identified as 3D assembly of interconnected CNTs with open and hierarchical pores (Du et al., 2015).

2.3.2.1. CNT aerogel

Among many techniques that have been adopted to synthesize highly functional and hybrid CNT aerogels (Fig. 4), a commonly used process starts by producing a gel filled with desired colloidal particles such as CNTs or graphene sheets, followed by extracting the liquid out of the gel structure via critical point drying (CPD). Jung et al. (2012) have synthesized the SWNT aerogels in this manner, where the homogenous dispersion of the solid phase at dilute concentration is firstly prepared, followed by supercritical drying of the solvent to finalize the aerogel structure (Fig. 4a). Aerogels have been also synthesized in a three–step process including (i) chemical assembly of CNTs in a solution and forming a stable gel with the aid of a cross–linker [e.g. ferrocene-grafted poly (p-phenyleneethynylene)], (ii) extracting the solvent by supercritical drying the solution in CO_2 to obtain the aerogel structure, and (iii) thermal annealing of the aerogel to improve the mechanical as well as electrical properties (Kohlmeyer et al., 2011).

2.3.2.2. CNT foam

The 3D monolith structures of CNT foams can be grown directly via CVD techniques on metal foams, followed by removal of the metal substrate to leave a 3D entangled CNT structure with macroporosities. These lightweight structures possess high sorption properties with low bulk density which are desirable properties for environmental cleanup applications, and can be further manipulated with functional groups and with the aid of many innovative synthesis techniques to produce hybrid materials with a wide range of applications (Fig. 5). Dong et al. (2012) synthesized the CNT–graphene foam via a two-step CVD process, where the graphene is first grown on nickel foam, followed by the CNT growth in CVD at 750 °C for 40 min, and overnight removal of the metal foam substrate with the aid of hydrochloric acid. The resulted structure exhibited super–hydrophobic properties, and further claimed to be applicable as a 3D highly conductive electrode for energy storage/conversion systems.

2.3.2.3. CNT sponge

CNTs have also been prepared as a self–assembled, interconnected network of highly porous (> 99%) sponges, with high surface area, stability, and flexibility. Various methods for synthesizing the CNT sponges have been developed over the years, enabling the production of composite sponges, as well as different arrays and orientation of CNTs in the sponge–based fabricated

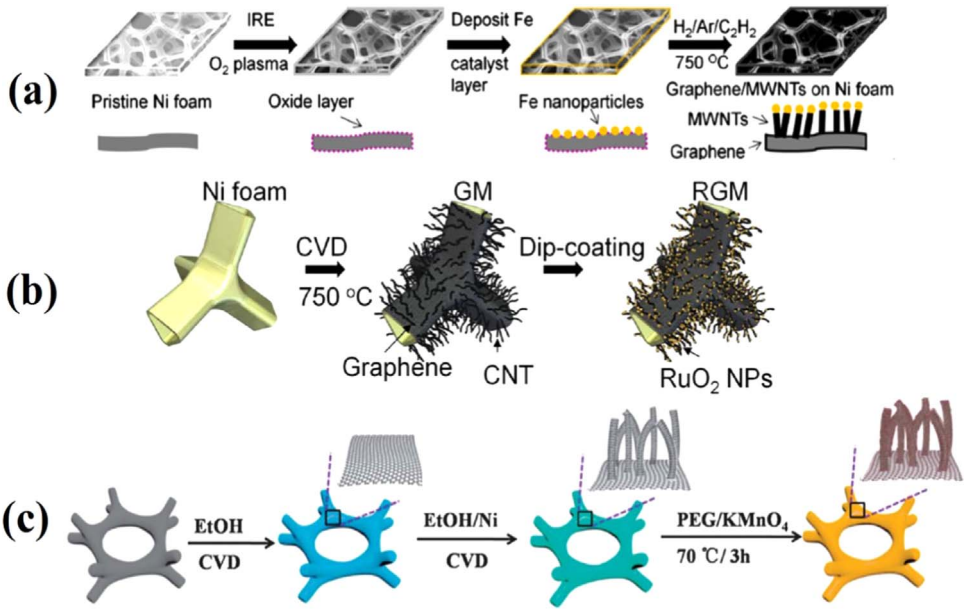

Fig. 5. Schematic illustration of the CNT–based foam synthesis process: (a) Growth and synthesis of graphene/MWCNT foam. Reprinted from Wang et al. (2013a), Copyright (2013), with permission from Elsevier. (b) Synthesis of the hydrous ruthenium oxide (RuO_2) anchored graphene and CNT hybrid foam (RGM). Reprinted by permission from Macmillan Publishers Ltd.: Scientific Reports (Wang et al., 2014a), Copyright 2014. (c) Synthesis of the MnO_2–CNT–graphene–Ni hybrid foam (EtOH means ethanol). Reproduced from Zhu et al. (2014) with permission of The Royal Society of Chemistry.

components (Fig. 6). Many variations of sponge-like CNT–based structures were introduced which are mainly synthesized via CVD process, however, the cost-effectiveness of such method of production still remains a concern when these structures are to be integrated into energy harvesting devices such as batteries and MFCs. A recent effort to address this issue involves the cost-effective (0.1 $\$/g_{CNT}$) synthesis of the CNT sponges in a single–step process within a three zone CVD furnace (Fig. 6a) (Erbay et al., 2015b).

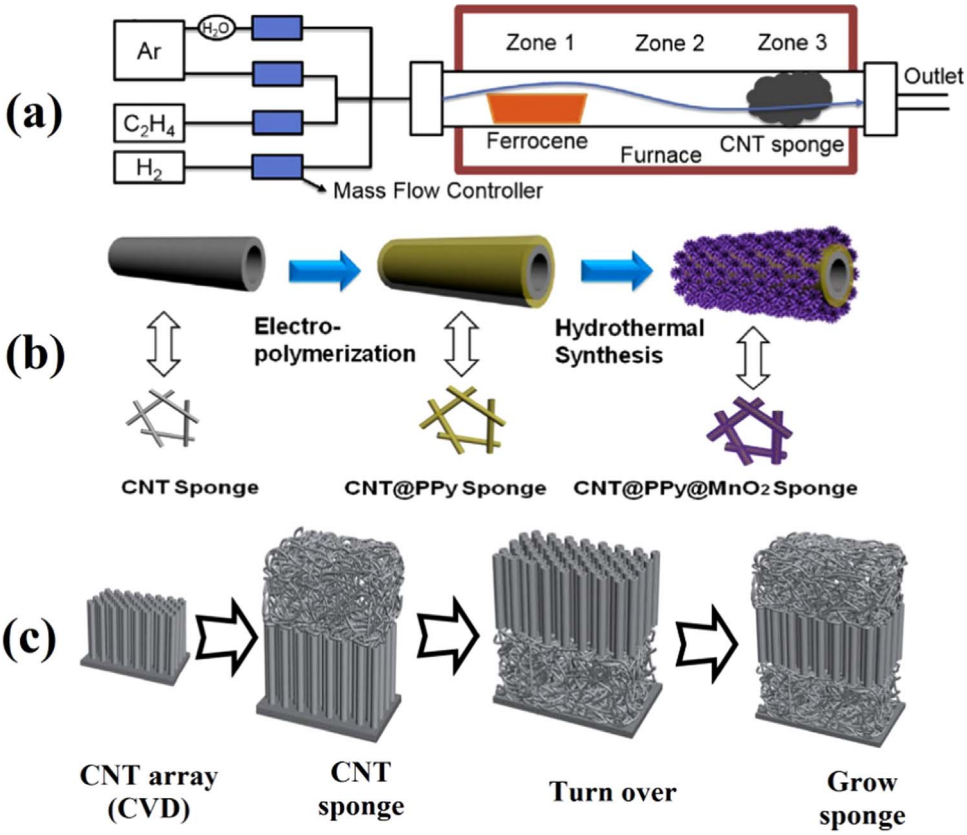

Fig. 6. Schematic illustration of the CNT–based sponge synthesis process: (a) Synthesis of CNT sponge electrodes inside a CVD furnace with three temperature controlled zones. Reprinted with permission from Gittleson et al. (2012), Copyright 2012, American Chemical Society. (b) Synthesis of MnO_2–PPy–CNT sponge via coating a PPy layer, followed by a hydrothermal process to attach the MnO_2 shell. Reprinted with permission from Li et al. (2014), Copyright 2014, American Chemical Society. (c) Growth of sponge–array–sponge structure with the aid of a multi–step CVD process. Reprinted with permission from Zeng et al. (2013), Copyright 2013.

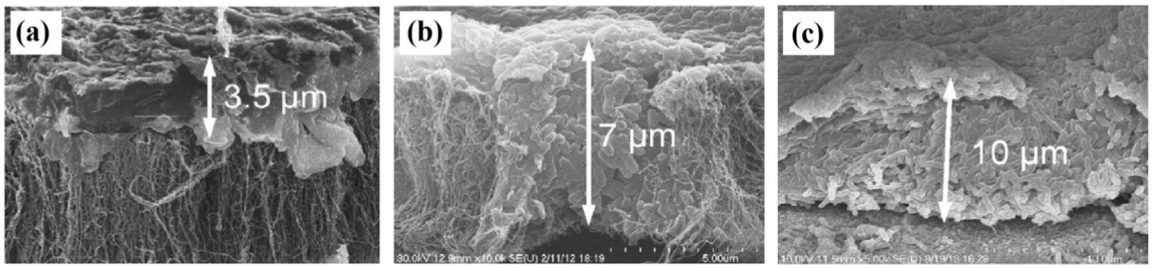

Fig. 7. SEM images showing the thickness of biofilm formed on (a) VACNT network or CNT forest, (b) RACNT network, and (c) spin–spray layer–by–layer (SSLbL) anodes. Sheet resistances of anode measured by a four–point probe technique are $1.48 \pm 0.004 \times 10^3$, $2.98 \pm 0.354 \times 10^3$, $3.84 \pm 0.17 \times 10^0$ Ωsquare^{-1}, for VACNT, RACNT and SSLbL networks, respectively. Reprinted from Ren et al. (2015), Copyright 2015, with permission from Elsevier.

3. Anode modification

An anode compartment acts as an electron generator and thus plays a major role in power output of the MFC. In this section we first attempt to identify the bacteria/electrode communication, as it is the key element for understanding pathways for anode improvement. Afterwards, we provide a review of the anode materials/structures that have been reportedly used to improve the MFCs overall performance.

3.1. Bacteria/electrode interaction

Exoelectrogenic bacteria, or electrochemically active microorganisms, which are responsible for converting biomass into electricity, live to a great degree in a self–produced polymeric matrix attached to the electrode surface, known as biofilm. Due to their complex nature, biofilms were studied from different aspects in terms of formation, growth and metabolic activity (Speers and Reguera, 2012), electron transfer mechanisms (Bonanni et al., 2012; Korth et al., 2015; Renslow et al., 2013), and environmental impacts (Kumar et al., 2013). Bacterial biofilms are the backbone of bacteria/electrode interaction, which develop via sequential steps: the process begins with bacteria surface attachment, followed by monolayer formation, multilayer formation, production of a polymeric scaffold, and eventually maturation of the biofilm towards forming a 3D structure (Romeo, 2008). This process can be regarded to take place in two periods of time; before and after biofilm maturation.

Before biofilm maturation the surface of the electrode should be a favorable place for the bacteria adhesion. This is highly regulated by the surface morphology, and can be enhanced with higher porosities, micro/nano–textures, hydrophilic substrates, and more biocompatible electrode materials. Due to the low surface density of the bacteria in this period, the MFC power output is very low, and often is a combination of the low electrocatalytic activity of the bacteria and presence of the electrolyte. In the second period, bacteria and electrode interact through a 3D multilayer biofilm, which largely impacts the cell viability and catalytic activity by regulating the mass diffusion of the substrate, and electron transfer mechanisms. In a multilayer biofilm, three pathways of electron transport have been known for a long time to take place at the proximity of the anode surface (Fig. 1); (i) electron shuttles in the bacterial environment that is reduced by the bacteria and oxidized at the anode surface, (ii) electron transfer via redox–active enzymes such as c–type cytochromes at the outer surface of bacterial cell membrane, and (iii) electron transfer mediated by self–produced electrically conductive pili known as bacterial nanowire. Often the direct mechanism of electron transfer (ii) is facilitated by micro/nano–textures with high electrical conductivity, and is more preferred due to its lower overpotential compared to other pathways.

3.2. CNT–based anode materials

Review of the recent advances in CNT–based MFC anodes shows that CNTs were extensively used as the backbone of various nanocomposites due to their high mechanical stability and electrical conductivity, and this has emerged as an attractive strategy to circumvent the restrictions, in terms of stability, toxicity, biocompatibility of inert CNTs. Generally, CNTs can be synthesized with natural polymeric matrices such as chitosan (Canavar et al., 2015), gelatin (Kavoosi et al., 2014), alginate (Sui et al., 2012), or collagen (Lee et al., 2014), synthetic polymers including polyurethanes (Tijing et al., 2013), polycarbosilane (Dalcanale et al., 2015), polycarbonate (Bautista-Quijano et al., 2016), poly (lactic–co–glycolic acid) (PLGA) (Zhao et al., 2013), poly (methyl methacrylate) (PMMA) (Ormsby et al., 2012), and/or decorated with metal oxide or metal catalyst nanoparticles. Exploiting these nanocomposites for the MFC anodes aims to pursue a more biocompatible anode with enhanced EET mechanisms of the bacterial community.

3.2.1. Polymer/CNT

A key element in biocompatibility of anodes composed of CNTs conjugated with a polymeric matrix is the sheet resistance which also contributes to the anode ohmic loss. Ren and coauthors (Ren et al., 2015) evaluated the biofilm formation on ultrathin CNT/polymer multilayers against the bare CNT electrodes and bare gold. Compared to the synthesized CNTs on a conductive substrate, CNT/polymer multilayer constructed using a spin–spray layer–by–layer (SSLbL) approach has shown an improved performance as the anode material. This can be ascribed to the lower sheet resistance of SSLbL electrodes that facilitates thicker biofilm formations as shown in Fig. 7.

Positively charged polymeric matrix might attract negatively active *exo*electrogens by electrostatic attraction, which might eventually enhance the active sites for short range EET mechanisms. This was observed by Nguyen and coworkers (Nguyen et al., 2013), where the use of mesoporous polysulfone matrix (MPPS) coated with SWCNT as the anode material of MFC enhanced the direct EET of bacterial community, and improved the anode performance. Moreover, with the aid of MPPS, this research group has constructed a mesoporous (~ 100 μm pore size) anode to avoid the mass transfer limitation and low active surface area associated with very small (< 10 μm) or very large (> 500 μm) porosities, respectively.

As aforementioned, CNTs can also be conjugated with natural polymers. In a recent study CNT hydrogels were prepared for MFC anode by first preparing a chitosan/CNT solution, followed by electrophoretically depositing the solution on a carbon paper (Liu et al., 2014). CNT hydrogel has been shown to facilitate electron transfer and bacteria/electrode communication, paving the way for higher current densities for oxidation reaction occurring at the anode. As a quantitative comparison, carbon paper coated with

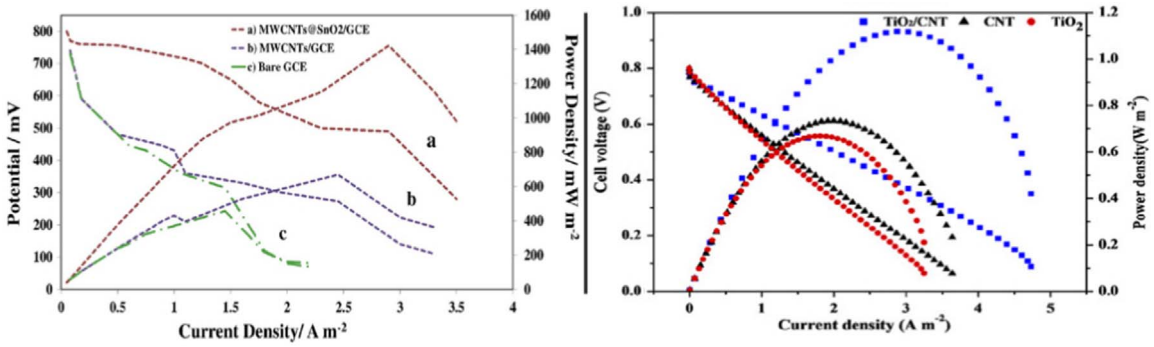

Fig. 8. Polarization and power density curves of MFCs improved by CNT–based anodes decorated with metal oxide. (Left) MFC Performance of MWCNT decorated with tin oxide (SnO_2) on glassy carbon electrode (GCE) as the anode material compared to bare GCE and MWCNT/GCE. Reprinted from Mehdinia et al. (2014), Copyright 2014, with permission from Elsevier. (Right) MFC performance of CNT decorated with anatase titanium oxide (TiO_2) as the anode material compared to the bare CNT and TiO_2 anodes. Reprinted from Wen et al. (2013), Copyright 2014, with permission from Elsevier.

hydrogel has shown 23% and 65% increase in current generation and maximum power density, respectively, compared to the case of using bare carbon paper. This opens up the potentials for applications of CNT hydrogel coated substrates as an easy–to–prepare, cost–effective, and highly porous candidate for MFC anodes.

3.2.2. Metal/CNT

Immobilization of metallic nanoparticles on CNTs as the scaffold has long been known to have several potential applications in sensors (Nayak et al., 2013), electronics (Vinoth et al., 2016), and fuel cells (Vinayan et al., 2012). Metal oxides including TiO_2, SnO_2, MgO_2, showing structural stability, low–cost, and abundance, are promising new materials to be integrated into CNTs or CNT/polymer hybrid materials. MFC anodes utilizing CNT–based material decorated with metal oxide nanoparticles have been shown to outperform those comprised of bare CNTs or metal oxides on a substrate. Wen et al. (2013) have applied anatase titanium oxide (TiO_2) nanoparticles synthesized with polymer modified CNTs as the anode material for MFCs. This nanohybrid material owning the characteristics of both TiO_2 and CNTs has outperformed CNT– and TiO_2 based electrodes in terms of biocompatibility, electrical conductivity, and surface properties (Fig. 8). Tin oxide (SnO_2) nanoparticles glued to CNTs have also been applied for MFCs electrode material. Mehdinia and coauthors (Mehdinia et al., 2014) evaluated a MFC anode composed of glassy carbon electrode coated with MWCNT decorated with SnO_2. On this basis, the MFC performance was significantly improved compared to the cases with MWCNT on glassy carbon electrode and bare glassy carbon electrode, as shown by the polarization curves in Fig. 8.

3.3. CNT–based anode assembly

Aside from the chemical properties of the CNT–based materials, the architecture of the anode largely regulates the MFC performance by controlling the mass diffusion, biofilm viability, and EET mechanisms. According to the recent literature, MFC anodes were structured as (i) thin films of CNTs or functionalized CNTs on a conductive support, (ii) self–assembled CNTs, and (iii) CNT–based monoliths/free–standing structures, which are covered in the followings.

3.3.1. Thin film structures

When synthesizing CNTs thin films, CNT alignment regulates many factors including porosity and sheet resistance that impact to a large extent the electrode biocompatibility in terms of mass transfer of nutrients, and biofilm formation and thickness. For instance, the porosity determines the extent to which the bacteria penetrate into the conductive network of CNTs, and nutrients are diffused into the layers of biofilm. CNTs can be glued onto a substrate to create an array of different surface architectures, including vertical alignment often called “CNT forest”, randomly dispersed, and entangled CNTs; few examples are shown in Fig. 9. Although potentially useful, these architectures have yet to be studied for their impact on bacteria electrocatalytic activities before being used as MFC anodes. Mink and colleagues (Mink and Hussain, 2013) used a silicon substrate within a CVD furnace to grow vertically aligned MWCNT on a catalyst bed to be used as the anode material. The selection of vertical alignment or “CNT forest” resulted in highly increased active area of the electrode due to the large SAV ratio of individual CNTs and porosity of the forest. On this basis, a membraneless air–cathode micro–MFC utilizing the

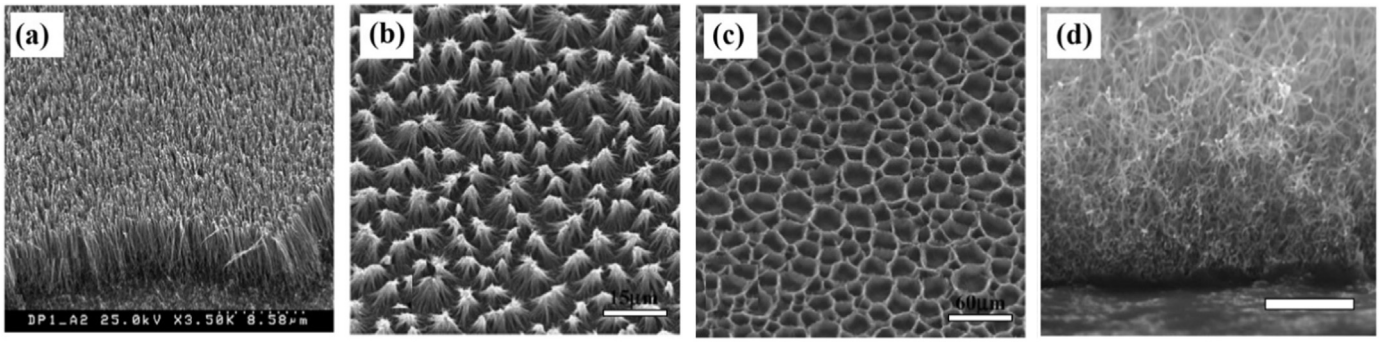

Fig. 9. SEM images of various surface architectures of CNTs. (a) Vertically aligned MWCNTs or CNT forest. Reprinted from Lobo et al. (2008), Copyright 2008, with permission from Elsevier. (b) Pyramid–like structure of MWCNTs (scale bar = 15 μm). (c) Cross–linked MWCNT forming cavities (scale bar = 60 μm). Reprinted with permission from Correa-Duarte et al. (2004), Copyright 2004, American Chemical Society. (d) Free–standing entangled CNTs (scale bar = 5 μm). Reproduced from Zhang et al. (2010) with permission of The Royal Society of Chemistry.

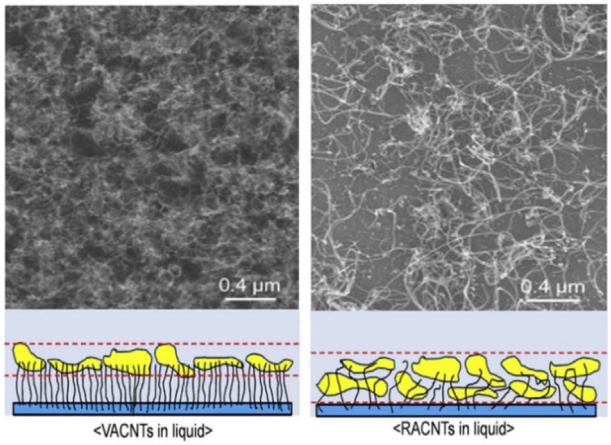

Fig. 10. Surface architecture of CNTs on a substrate of quartz. (Left) Synthesized CNT in a vertical alignment (CNT forest or VACNT), SEM image of the resulting anode surface, and the effect on bacteria adhesion most of which remain at the tip of the CNTs. (Right) Randomly synthesized CNTs (RACNT), SEM image of the anode surface, and bacterial growth within the CNT network that displays cell adhesions in larger quantity and thus more biocompatibility compared to the CNT forest. These improvements can be ascribed to a larger pore size of RACNT network. Reprinted from Ren et al. (2015), Copyright 2015, with permission from Elsevier.

modified anode was shown to be a high endurance energy harvester that reached current and power density of 6 and 20 times, respectively, higher than conventional gold and nickel electrodes. For the first time, these findings provide routes for sustainable on–chip power production with a MFC to be utilized in electronics or ultra–low power devices.

The pore size of various surface alignments of CNTs also impacts the bacteria accommodation within the CNT network, cell viability, and biofilm formation. Ren and others (Ren et al., 2015) included in their study the comparison between highly porous features with vertically aligned CNTs (VACNT) or CNT forest, randomly aligned CNTs (RACNT), and spin–spray layer–by–later (SSLbL) CNT films on the gold substrate. The results of the study validated that VACNTs might in fact impede the bacterial penetration into the CNT network and reduce the cell adhesion compared to RACNTs (Fig. 10). As discussed in (Ren et al., 2015), VACNT forest resists the mechanical force exerted by the bacteria, thereby lowering the active area for mass transfer of nutrients and electron conduction which is often followed by thin biofilm formations. In contrast, easy accommodation of bacteria within the RACNT network paves the way for thicker biofilms and thus higher electricity generation.

As aforementioned, individual CNTs are known to have a very high SAV ratio with a length that could achieve up to millimeters. It is evident that longer CNTs increase the probability of cell adhesion to the CNT network that can positively influence the anode performance. To investigate the impact of CNT length, Erbay and coworkers (Erbay et al., 2015a) have tested anodes of CNTs with three different sizes ranging approximately between 8 μm and 19 μm that are loosely packed onto a stainless steel (SS) mesh. Instead of applying polymeric binders, using direct growth of CNTs to SS mesh reduces anodic ohmic loss. The results of the study showed a 28% improvement in MFC power density when switching from the short CNT network to the long CNT network, as shown in Fig. 11.

3.3.2. *Self–assembled structures*

Instead of bonding a CNT network onto a substrate, CNTs can be directly dispersed into the anolyte to form a 3D conductive network so as to increase to a maximum level the active surface area for bacterial adhesion and biofilm growth. This approach opens up the potential to enhance the contact based electron transfer, and possibly increases to a great degree the extent of nutrition supply to the bacterial biomass. Matsumoto et al. (2014) adopted this approach for a two chamber MFC separated by a membrane (Fig. 12). To generate the 3D conductive network, concentration of CNTs simply dispersed without the aid of any dispersant should meet the percolation threshold. The percolation theory determines the volume fraction of CNTs in a solution after which CNTs start forming a network by attaching to each other. The resulting entangled conductive CNT network can be assembled onto a carbon based anode. However, this approach might necessitate the use of a membrane which negatively influences the sustainability of energy production, power output, and device cost.

3.3.3. *Monolith structures*

Most techniques devised to generate 3D electrodes by synthesizing CNTs with nanoparticles require support materials, such as carbon paper, carbon cloth, textile, and stainless steel mesh. Gui and coauthors (Gui et al., 2010) reported the synthesis of CNT

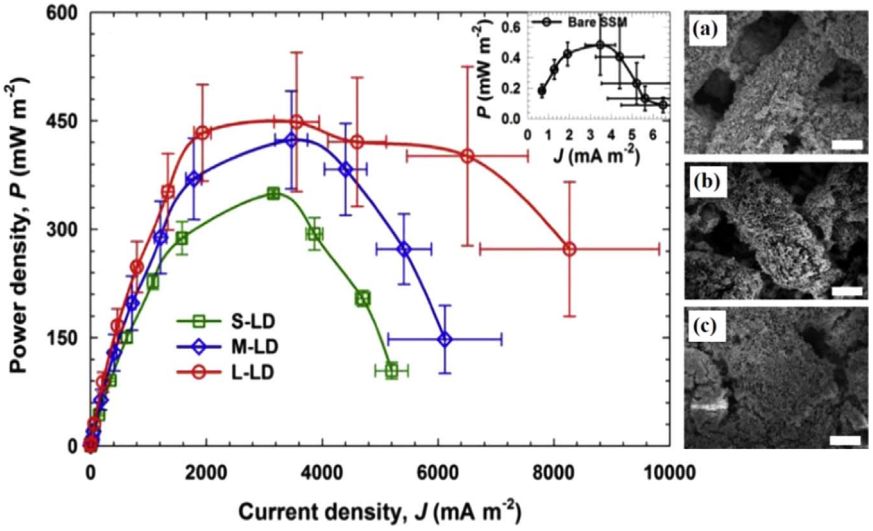

Fig. 11. The effect of CNT length on MFC current and power density. (Left) Power density versus current density for short CNTs or S–LD (~8 μm), intermediate CNTs or M–LD (~13 μm), and long CNTs or L–LD (~19 μm), where LD stands for "low density" referring to the packing density of CNTs synthesized onto stainless steel (SS) substrate. (Right) SEM images of (a) S–LD (b) M–LD (c) L–LD, where the scale bars are 20 μm. Reprinted from Erbay et al. (2015a), Copyright 2015, with permission from Elsevier.

sponge which is a self–assembled interconnected network of individual CNTs without support materials. Reportedly, the sponge has shown attractive properties, including very low density, high porosity (99%), high structural flexibility, and high absorption capacity, thus it has recently been applied for environmental cleanup, filters, compressible foams (Gui et al., 2011, 2010; Li et al., 2010).

Conventionally, carbon felt and carbon brush were used as a 3D anode material for MFCs, which enhance cell adhesion, owning to their 3D structure and large SAV ratio. An alternative for these 3D electrodes is the porous spongy scaffolds coated with CNTs. Chou et al. (2014) have tested melamine sponges coated with the reduced graphene oxide (rGO)/CNT as the anode material for MFCs. Due to the high mass transfer of nutrients through the 3D porous melamine scaffold, the anode has shown excellent biocompatibility for *Escherichia coli* (*E. coli*) proliferation and metabolic activities compared to the traditional carbon paper and metal based electrodes. Such biocompatibility enables long lasting operation cycles of the MFC, as shown in Chou et al. (2014) where they achieved a 20 days successful operating period. More recently, the CNT sponge has shown to be a promising 3D CNT–based electrode material that offers highly enhanced electrical conductivity compared to its conventional counterparts. Erbay et al. (2015b) recently synthesized a 3D flexible CNT sponges as a stand–alone material for MFC anode, which has shown superior performance over the 3D carbon felts: 13 times lower charge transfer resistance, and 40% larger power density, as well as scalable and low–cost synthesis of CNT sponges, thereby providing routes for commercialization of MFCs. In future, CNT sponges can be used as a scaffold for redox polymers or metal and metal–oxide nanoparticles in the pursuit of fully functionalizing their properties.

In sum, the performance of various CNT–based materials, including the methods of assembly and architecture were summarized in Table 1. Note that despite the paramount importance of the anode material and its surface architecture, many elements contribute to the power output of the MFCs, including the electron acceptor/donor that determines the theoretical half–cell potentials, cathode materials for the ORR mechanism, and MFC size that impacts the internal ohmic resistance.

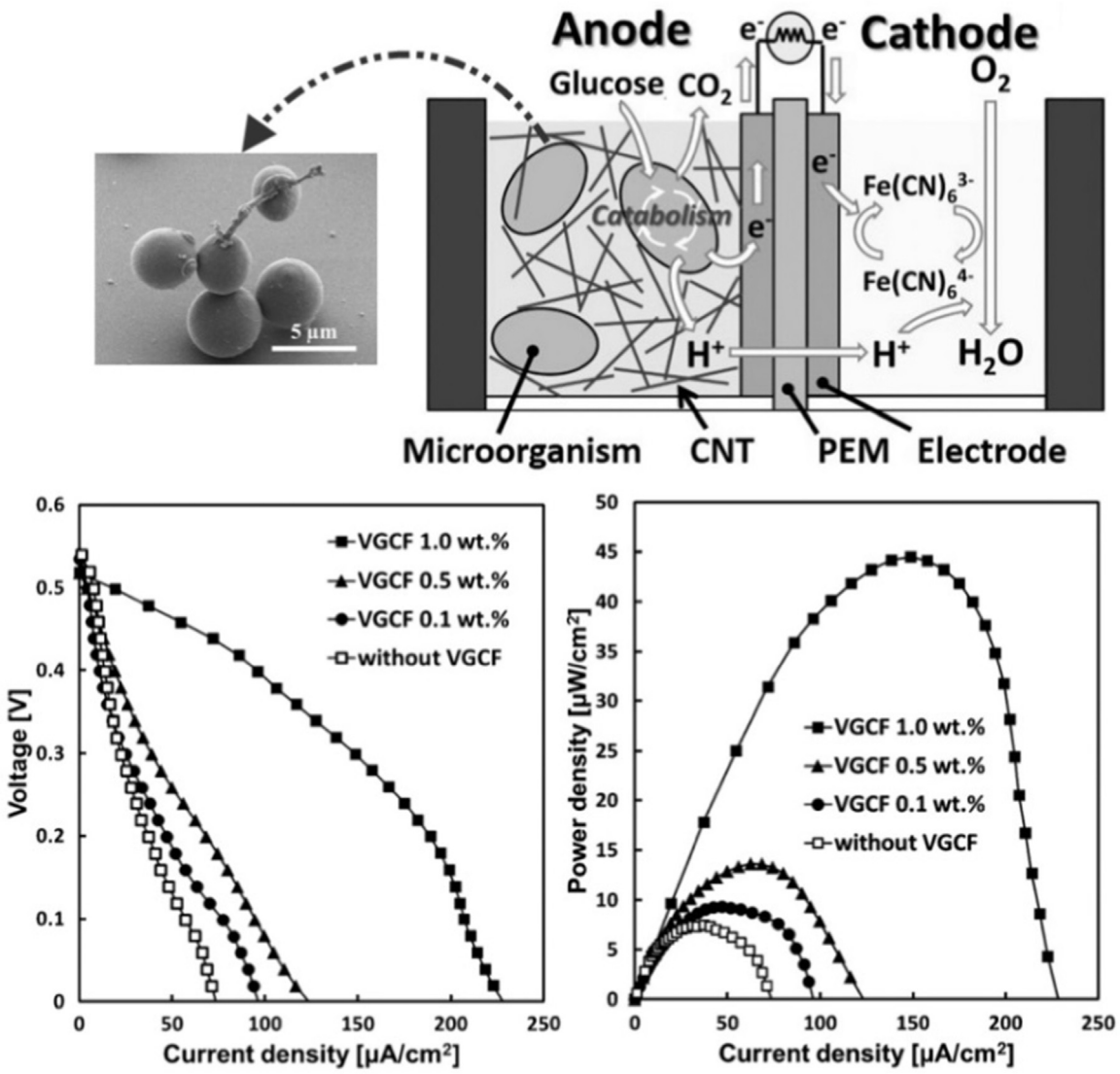

Fig. 12. (Top left) SEM image of CNTs adhered to *Saccharomyces cerevisiae* cells and (Top right) schematic of the 3D conductive network of CNTs used in the anode solution of MFC. (Bottom left) Polarization and (Bottom right) power density curves of MFC, showing an approximately maximum 8– and 25–fold higher current and power density, respectively compared to the case without CNT dispersion. Reprinted with permission from Matsumoto et al. (2014), Copyright 2014, AIP Publishing LLC.

4. Cathode modification

The cycle of power generation in a MFC is completed when the electron acceptor, mostly oxygen, is reduced at the interface of cathode, oxygen, and electrolyte, as a result of which water is produced. Normally, ORR kinetics is very slow, demanding the search for catalysts and their support materials that could enhance the active area for oxygen adsorption and increase the exchange current density. Differences between catalytic activities of materials towards reducing the electron acceptor might stem from the overall electron transfer for the surface reactions. Easier electron transfer is often accompanied with higher catalytic performance and lower activation energy. Conventionally, precious metals such as platinum (Pt) were preferred mainly due to their high electrocatalytic activity towards ORR. However, in the case of Pt cost and lack of stability of commercially available carbon–black supported Pt fueled the search for alternatives including noble metals, non–noble metals, metal oxides, carbon materials, and alloys.

Over the years CNTs and functionalized CNT networks were used as either the catalyst, or a durable scaffold for catalysis due to their possible reactivity towards ORR and superior mechanical stability. From a general standpoint, CNT scaffolds prevent detachment of catalyst, which otherwise aggregates in certain points, causing a disturbance in surface reactions and overall performance of the electrode. Moreover, either functionalization of CNTs or the chemical attachment of organic (proteins, enzymes, polymers, etc.) and inorganic (metal, metal oxides, etc.) functional groups, eventually enriches the CNTs with high catalytic activity towards ORR (Gao et al., 2012).

The ORR slow kinetics is a major setback for many industrial applications, such as the fuel cell and battery industry, thus attentions are given to the development of catalysts that can improve energy conversion efficiency in lithium–air batteries (Christy et al., 2015; Wang et al., 2012) as well as acidic and alkaline fuel cells (Kruusenberg et al., 2012; Shui et al., 2015; Xiao et al., 2015). However, the integration of such catalysts into MFC cathodes is quite questionable, as their good performance towards ORR is to be verified in the biocompatible environment provided for bacterial metabolism and viability that requires low antibacterial effects, and operation at virtually neutral electrolytes and room temperature. In this section we first begin with identifying the role of carbon materials in the mechanism of oxygen reduction, and then we delineate the methods devised to reduce or eliminate the use of traditional Pt loaded cathodes that could impact the cost–effectiveness and efficiency of bioresource energy recovery in MFCs.

4.1. Oxygen reduction mechanism on CNTs

The cathodic ORR mechanism is quite complicated and often consists of intermediates that can be determined by experimental techniques. Two general pathways of oxygen reduction to water (H_2O) are often examined to assess the catalytic activity of the cathode: direct reduction to H_2O through a 4–electron pathway, and indirect reduction through 2–electron pathways with hydrogen peroxide (H_2O_2) as the intermediate, with the former pathway being favored, as it provides higher energy conversion efficiency. Generally in carbon materials the catalytic activities towards ORR are attributed to the presence of quinone functional groups (Yeager, 1986), which has also been ascribed to the reduction mechanism at CNTs surfaces (Zhang et al., 2004). Due to the high SAV ratio and defect–rich surface of functionalized CNTs, CNT–based materials have the potential to facilitate the ORR mechanism, and enhance the adsorption sites for oxygen. However, in more complex nanoengineered surfaces, the ORR mechanism may vary widely depending on the type of carbonaceous material and chemical functional groups that may lead to the formation of H_2O_2, OH^-, or a mixture of both. To better understand the ORR mechanism and develop non–precious catalysts, attentions were given to the composition and structure of active sites on CNT–based materials. For instance, Rao et al. (2010) investigated the structure of the ORR sites on vertically aligned CNTs doped with nitrogen containing groups, and found that the pyridine–type nitrogen sites may be responsible for the good electrocatalytic activity of the nitrogen–doped CNTs (N–CNTs).

4.2. CNT–based cathode materials

Recent progresses in MFC cathode modification demonstrate the widespread use of electrodes loaded with CNTs functionalized with chemical groups, metals/metal oxides, polymers, or a combination of both, which are discussed in the followings.

4.2.1. Pre-functionalized CNTs

Oxidation of CNTs by having oxygen–bearing functionalities such as carboxyl and hydroxyl groups introduced to the CNT structure enables easier attachment of CNTs onto other materials, creates surface defects for higher catalytic activity, enhances the active sites for ORR, provides better dispersion of catalysts, and improves CNTs solubility in the polymer matrix. Oxidative treatment is often accompanied by boiling the CNTs in a solution of sulfuric acid (H_2SO_4), nitric acid (HNO_3), or a mixture of both. Different substrates such as carbon felt, glassy carbon electrode, and metal coated silicon wafers, can be then coated with functionalized CNTs and used as MFC cathode. Zhu et al. (2015) electrophoretically deposited the acid–treated MWCNTs on graphite felt for use in sediment MFC, and achieved approximately 60% higher power density than bare graphite felt cathode. Lu et al. (2013) have shown that the HNO_3 treatment increases the conductivity of pristine CNTs by nearly 60%, which may utterly improve the electrocatalysis ability of the cathode. The survey of cyclic voltammetry (CV) of this cathode has also shown an increase in ORR peaks, highlighting the importance of CNT pretreatment before being hybridized with other functional groups. Ghasemi et al. (2013) have also functionalized inert CNTs in the mixture of sulfuric and nitric acid, showing its improved ORR catalysis compared to conventional carbon paper. Liew et al. (2015b) have also showed that the acid treatment in a mixture of sulfuric and nitric acid improves the catalytic activity of CNTs towards ORR. In addition, they showed that the functionalized CNTs tend to remain homogenous for a longer time compared to the pristine CNTs dispersed in ethanol. As aforementioned this is ascribed to the attachment of hydroxyl and carboxyl groups to the CNT structure after acid treatment.

Nitrogen–doped CNTs (N–CNTs) have also shown great promise to produce highly activated CNT–based catalysts for the improvement of sluggish ORR kinetics. The inclusion of nitrogen imposes a non–uniform charge distribution on the CNT surface, allowing easier adsorption and interaction with the oxygen (Wong et al., 2013). He et al. (2016) grew vertically aligned nitrogen-doped CNTs on carbon cloth to improve the ORR in MFC cathodes. The 3D vertical forest of N–CNTs has shown to enhance the active sites for electrolyte and oxygen adsorptions, lower the resistance, and improve the mass transfer and electrochemical performance towards a facilitated ORR pathway. This low–cost cathode for MFCs enhanced the MFC power density by 8.6% compared to the conventional Pt loaded cathodes. Similarly, Feng et al. (2011) studied the use of N–CNTs for catalysis in MFC cathodes, and achieved ~14% higher power density compared to the commonly used Pt loaded electrodes. Rotating ring–disk electrode (RRDE) and cyclic voltammograms shown in Fig. 13, describe in more details the impact of nitrogen containing groups on catalytic activities of electrodes compared to Pt catalyst. The cyclic

Table 1
Summary of the CNT–based anode performance.

Anode		**Cathode**	**Type**			**Max. power density ($\sim$mW m^{-2})**	**Refs.**
Coating/Support	Architecture/Method	Coating/Support	Microorganism	Electron donor/ acceptor	Configuration		
CNT/Carbon paper	3D conductive network/ Dispersion	None/Carbon paper	*S. cerevisiae*	Glucose/ Ferricyanide	Dual-chamber	1760	(Matsumoto et al., 2014)
CNT sponge/None	Sponge/CVD	Pt/Carbon cloth	Mixed	Acetate/ Ferricyanide	Dual-chamber	2150*	(Erbay et al., 2015b)
MWCNT/Silicon	Vertically aligned/Plasma enhanced CVD	Pt+PTFE/NA	Mixed	Acetate/Oxygen	Single-chamber	19.36	(Mink and Hussain, 2013)
MWCNT+SnO_2+PTFE/GCE	None/Drop casting	Pt/None	*E. coli*	Glucose/ Ferrocyanide	Dual-chamber	1421	(Mehdinia et al., 2014)
CNT+Mo_2C+PTFE/Carbon felt	None/Pressure coating	Polyethylene CEM+Pt+PVDF+NMP/ Carbon paper	*E. coli*	Glucose/Oxygen	Single-chamber	1050	(Wang et al., 2014b)
PSS+MWCNT+PVA/Gold–coated glass	Layer by layer/SSLbL	Cr+Au/Glass slide	Mixed	Acetate/ Ferricyanide	Dual-chamber	3320	(Ren et al., 2015)
CNT+TiO_2+Nafion/Carbon cloth	None/Drop cast	None/Carbon brush	Mixed	Acetate/ Ferricyanide	Dual-chamber	1.12	(Wen et al., 2013)
SWCNT/MPPS	None/Dip coating	Carbon cloth	*S. oneidensis*	Lactate/Ferricyanide	Dual-chamber	1410	(Nguyen et al., 2013)
CNT+Au+TiO_2/Carbon paper	None/NA	Pt+TiO_2/Carbon paper	*E. coli*	Glucose/Oxygen	Single-chamber	2.4	(Wu et al., 2013)
CNT+Chitosan/Carbon paper	None/Electrodeposition	Pt/Carbon cloth	Mixed	Acetate/Oxygen	Dual-chamber	132	(Liu et al., 2014)
MWCNT+MnO_2+Nafion/Plain graphite	None/Pressure coating	None/Graphite	Mixed	Marine sediment/ Oxygen	Single-chamber	109.1	(Fu et al., 2014)
MWCNT+PANI/Graphite felt	None/Electrodeposition	None/Carbon cloth	*S. putrefaciens*	Acetate/ Ferricyanide	Dual-chamber	257	(Cui et al., 2015)
MWCNT/SSM	NA/CVD	Pt/Carbon paper	*S. oneidensis*	Acetate/ Ferricyanide	Dual-chamber	450	(Erbay et al., 2015a)

PTFE: Polytetrafluoroethylene; CEM: Cation exchange membrane; PVDF: Polyvinylidene fluoride; NMP: N-Methyl-2-pyrrolidone; PSS: Poly(styrenesulfonate); PVA: Polyvinyl alcohol; PANI: Polyaniline; SSM: Stainless steel mesh.

* The unit is mW m^{-3} based on anode volume.

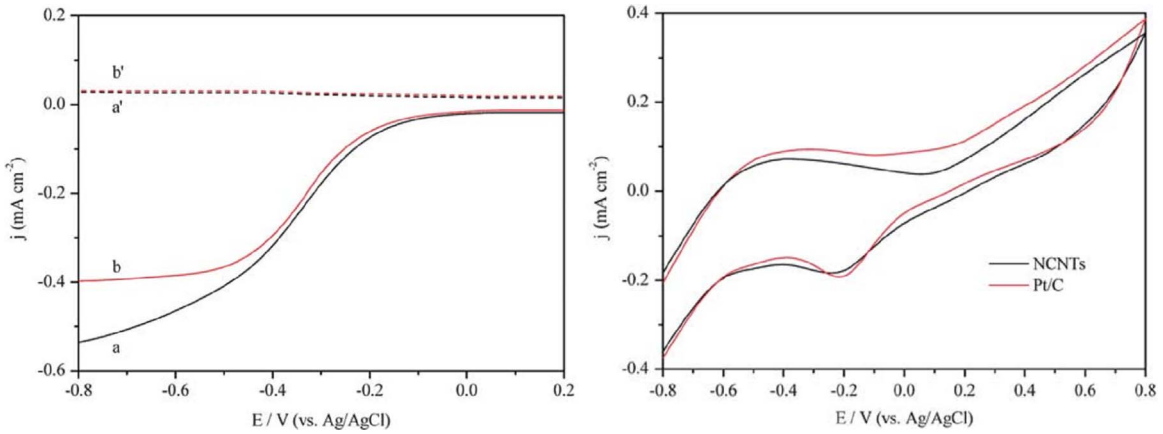

Fig. 13. (Left) RRDE voltammograms at 1000 rpm in oxygen saturated buffer, where the black and red line refers to the N–CNTs and Pt catalysts, respectively. (Right) Survey of cyclic voltammetry in oxygen saturated buffer solution, where NCNTs, and Pt/C refers to the use N–CNTs and Pt catalysts, respectively. Reproduced from Feng et al. (2011) with permission of The Royal Society of Chemistry. (For interpretation of the references to color in this figure legend, the reader is referred to the web version of this article.).

voltammograms exhibit similar electrochemical activity of N– CNTs compared to Pt, and the RRDEs suggest a 4–electron pathway reduction mechanism. These studies open up potential for the use of metal–free and non–precious cathodes for MFCs.

4.2.2. Metal /CNT

Traditionally Pt deposited onto the carbon–supported substrate, such as carbon paper, glassy carbon electrode, carbon felt, have been tested for use in the cathodic reaction of MFCs. On the other hand, due to the ability of CNT arrays to enhance the oxygen adsorption by increasing the active area for surface reactions, they are potentially useful as support material of metal catalysts. Halakoo et al. (2015) synthesized Pt/CNT nanocomposites and tested various cathodes by adjusting the amount of Pt conjugated with the CNTs. The results of MFC performance showed great promise for unloading precious metals from the cathode while virtually maintaining the same performance. Many researchers have also hybridized non–precious metal oxide with CNT arrays to compensate for the low electric conductivity of metal oxides when used as MFC cathode. Liew et al. (2015b) synthesized manganese (II) oxide (MnO) with functionalized CNTs to ease the charge transfer at the cathode and, in turn, the ORR mechanism. The resulting performance of the MFC has shown approximately 100% and 18% improvement compared to CNT, and functionalized CNT cathodes, respectively (Fig. 14). Similarly, manganese (I) oxide (Mn_2O) has also been investigated in a vertical array of CNTs grown on SS mesh. The results showed promising improvement compared to plain SS mesh that has high SAV ratio for oxygen adsorption in ORR (Amade et al., 2015). Nickel oxide (NiO) conjugated with CNTs has also been tested for catalytic activity towards ORR. The findings demonstrated superb catalytic performance of NiO/CNT composite compared to NiO, highlighting the importance of CNT array in MFC cathodes (Huang et al., 2015a). Stainless steel (SS) mesh have also been hybridized with CNTs to be used as the cathode of MFC. Zhang et al. (2013b), compared oxygen reduction on SS mesh and CNT/SS mesh, and then put the both electrodes into test as MFC cathodes; the findings demonstrated 49 times increase in power density when bare SS mesh was replaced by the CNT/SS mesh cathode. Similarly, Song et al. (2013) investigated SS mesh coated with MWCNTs as the MFC cathode, and the resulting power density of the MFC was improved by more than 300% compared to the case of bare SS mesh cathodes.

4.2.3. Polymer/CNT

The synthesis of polymer/CNT composites often involves the physical adsorption of polymers onto the CNT surface, or establishment of a strong interaction (covalent bonding) between the polymer chains and CNT structure. In the first approach the fabrication route is simply wrapping the CNTs with polymer chains. As to the second approach, the strong interaction between the CNTs and the polymer are achieved via in situ polymerization of monomers, or the chemical attachment of the polymer chains to the CNT surfaces. In situ polymerization is a highly flexible route for grafting the polymers to the CNTs with high density, and is enabled by the initiators attached to the defect–rich surface of oxidized CNTs. On the other hand, the monomers can be first polymerized into macromolecules, and subsequently attached to the CNT surfaces. While allowing the use of many commercial polymers available, this method is hindered by the steric impact of macromolecules and low reactivity of polymer chains when they need to attach the CNT surface (Lou et al., 2004; Riggs et al., 2000; Spitalsky et al., 2010; Wu et al., 2003). Among many commercially and custom–made polymers, conductive polymers [e.g., polypyrrole (PPy) and polyaniline (PANI)] exhibiting environmental stability and easy synthesis with CNTs were also tested as MFC cathodes. Ghasemi et al. (2015) have studied the catalytic activity of PPy/CNT for use as MFC cathode, and evaluated the performance with respect to Pt electrodes. Although showing less catalytic activity towards ORR compared to Pt electrodes, this nanocomposite is a promising alternative of MFC cathode in that it is cost–effective and only leads to ~8% reduction in power density of the MFC, while increasing the current density by ~4%.

4.2.4. Metal/polymer/CNT

Even though metal oxides have shown catalytic activity towards ORR, they possess poor electrical conductivity. Therefore, their combination with conductive polymers (e.g., PPy and PANI), and the highly conductive networks of CNTs may improve the exchange current density and catalytic performance. On the other hand, polymers may also be constrained by low conductivity and their application as bare MFC electrodes arises many concerns in terms of charge transfer. With that being mentioned, the metal/polymer/CNT composites are potential candidates to provide a highly conductive network for exchange of the charges and oxygen adsorption, and thus they are expected to enhance the catalytic activity of MFC cathodes. For example, Lu et al. (2013) synthesized Mn/PPy/CNT composite as a cost–effective air–breathing cathode for MFC which has comparable catalytic activity with traditional Pt coated on carbon black, and may open up potential for scaling up the energy recovery using MFCs (Fig. 14).

In sum, Table 2 provides overview of the recently reported MFC cathodes based on CNTs and CNT hybrid materials. Note that, here

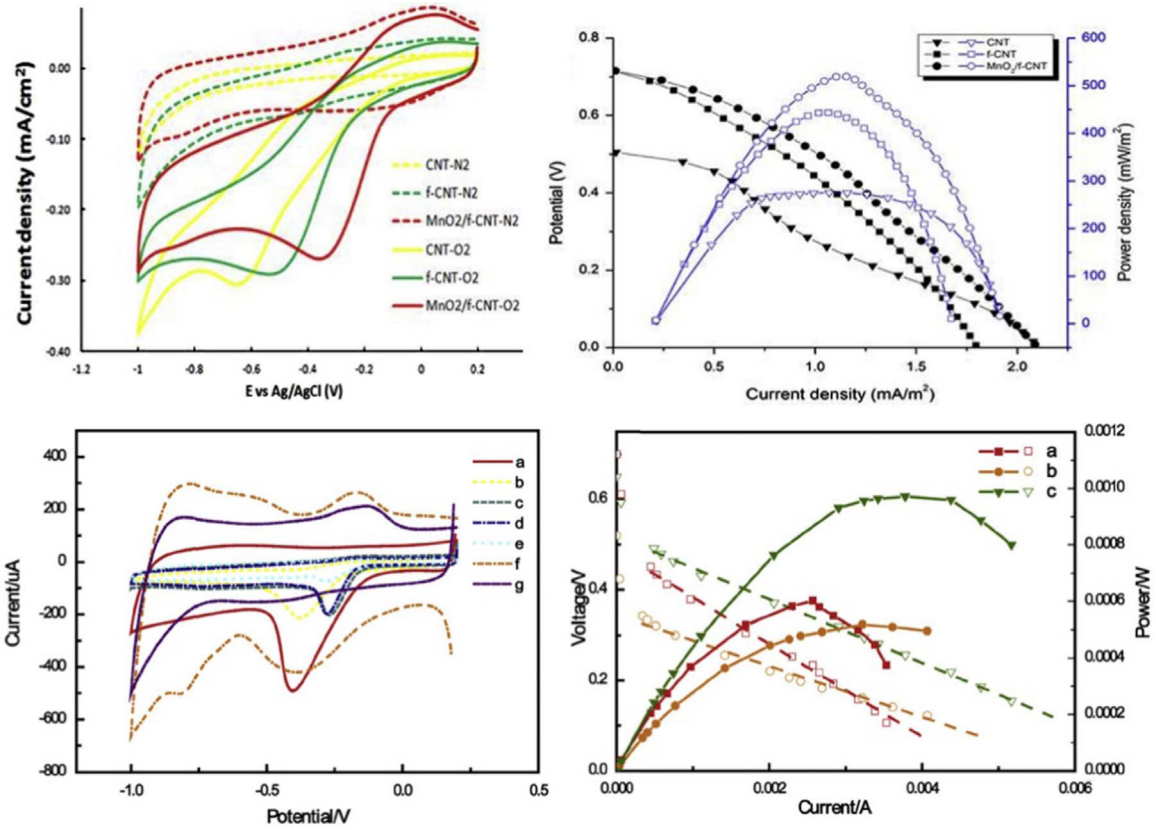

Fig. 14. Top row: (Left) CV curves of CNT–based cathodes, and (Right) power density curves of the MFC. Reprinted from Liew et al. (2015b), Copyright 2015, with permission from Elsevier. Bottom row: (Left) CV curves of cathodes composed of (a) Mn/PPy/CNT, (b) Mn/CNT, (c) PPy/CNT, (d) HNO_3–treated CNTs, (e) raw CNTs, and (f,g) Pt (0.5 mg cm^{-2})/carbon black; (a-f) and (g) are operated in aerobic and anaerobic condition, respectively. (Right) Power density curves of the MFC; (a) Mn/PPy/CNT (2 mg cm^{-2}), (b) Mn/PPy/CNT (1 mg cm^{-2}), (c) Pt/carbon black. Reprinted from Lu et al. (2013), Copyright 2013, with permission from Elsevier.

we excluded the use of biocathodes as the catalyst for ORR mechanism.

5. Challenges and promises

Over the years, innovations in CNT nanoengineered materials have brought explosive growth in the techniques of production and synthesis of nanocomposites for applications including energy storage/conversion devices. Laser–ablation and arch–discharge have been replaced by variations of CVD methods for industrial–scale of CNT production, and less sophisticated microwave–assisted synthesis facilitated in terms of time and cost the lab–scale research on CNT–based composites. With these efforts in the CNT industry, the price of MWCNTs have decreased from 45,000 to 100 $\$kg^{-1}$ (Zhang et al., 2013a), and if this trend continues to advance, the nanoengineered CNT materials may replace for commercial uses other carbonaceous or precious materials. In MFCs, for instance, the use of CNTs and functionalized CNTs was able to completely eliminate the need for expensive noble metal catalysts (e.g., platinum) for oxygen reduction at the cathode (Feng et al., 2011; Qu et al., 2010; Yang et al., 2011).

Many applications such as energy recovery during wastewater treatment require the scaling up of MFCs, and efforts were made to enlarge and stack such systems both in the laboratory and pilot–scale tests (Logan, 2010). Clearly, the scaling up techniques require fast, facile, and low–cost fabrication routes to make bioresource energy recovery more economically appealing for industry. CNTs, in this aspect, may contribute to resolve the issue of electrode surface area and ohmic losses by introducing highly porous electrode structures that not only offer superb electrical conductivity, but also increase the specific surface area of the electrodes for the enhancement of catalytic sites in both cathode and anode sides. Aside from bulky MFC units for large–scale energy conversion, miniaturized MFCs that are improved with CNTs may also find potential applications in many commercially available lab–on–a–chip devices such as micromixers (Yazdi et al., 2014, 2015a, 2015b), microsensors (Journet et al., 1997; Jung et al., 2012; Kabiri et al., 2014; Li et al., 2012), separators (Ahn et al., 2015; Brewer et al., 2014; Rao et al., 2015), micropumps (Amirouche et al., 2009; Urbanski et al., 2006), and low and ultra–low power electronics (Shenghua and Nanjian, 2007; Xu et al., 2014).

Clearly the CNT–based composites have enhanced the power density (Tables 1 and 2) compared to the more traditional counterparts such as carbon cloth, carbon paper, and metal–based electrodes; CNTs have caused major catalytic improvements in both cathodic and anodic reactions which helps to shrink the gap between theoretical and practical limits for bioenergy extraction from organic compounds. Despite these promising results, however, questions still remain about the antibacterial effect of these newly introduced nanocomposites that may negatively influence the cell voltage during long operating cycles. Moreover, our study shows that compared to other nanoengineered graphene–based electrodes, the CNT–based MFC electrodes still suffer from lower catalytic performance especially in the cathodic ORR mechanism (Table S1 and S2 in the Supplementary material). This suggests that more works dedicated to the use of CNT–based material in MFC cathodes are needed. For instance, the use of CNTs to modify the biocathodes based on either bacterial biofilms or biomolecules (e.g., enzymes) has yet to be studied in more depth, as they are good candidate to replace precious metal catalyst such as Pt.

Table 2
Summary of the CNT–based cathode performance.

Cathode side		Anode side	Type			Max. power density ($\sim mWm^{-2}$)	Refs.
Coating/Support	Architecture/Method	Coating/Support	Microorganism	Electron donor/acceptor	Configuration		
CNT/SSM	None/Dip coating	None/Graphite felt	Mixed	Acetate/Oxygen	Single- chamber	147	(Zhang et al., 2013b)
CNT + Pt/Carbon paper	None/Dip coating	None/Carbon paper	Mixed	Glucose/Oxygen	Dual-chamber	169.7	(Ghasemi et al., 2013)
Mn + PPy + CNT + Nafion/GCE	None/Drop casting	None/Carbon cloth	Mixed	Acetate/Oxygen	Single-chamber	213	(Lu et al., 2013)
MnO_2/ + CNT/Carbon paper	None/Brush coating	None/Carbon paper	Mixed	Mixed/Oxygen	Dual-chamber	520	(Liew et al., 2015a)
MWCNT/Graphite felt	None/Electrophoretic deposition	None/Graphite felt	Mixed	Sediment/Oxygen	Single-chamber	214.7	(Zhu et al., 2015)
CNT + PPy/Carbon paper	NA	None/Carbon paper	Mixed	Glucose/Oxygen	Dual-chamber	113.5	(Ghasemi et al., 2015)
NiO + CNT + Nafion/Carbon paper	None/Carbon cloth	None/Carbon felt	Mixed	Glucose/Oxygen	Single-chamber	670	(Huang et al., 2015a)
MnO_2 + CNT/SSM	None/PECVD	None/SSM	Mixed	Acetate/Oxygen	Single-chamber	24	(Amade et al., 2015)
N–CNT/Carbon cloth	Vertically aligned/CVD	None/Carbon cloth	Mixed	Acetate/Oxygen	Single-chamber	135	(He et al., 2016)

6. Conclusions

In this review article we turned our attention to the modification of MFC electrodes by taking advantage of CNTs and CNT composites that have been extensively validated to own unique characteristics compared to their conventional counterparts. High SAV ratio and electrical conductivity are the pivots of CNT–based material properties, causing them to positively influence the MFC performance. CNT–based modification in the anode side improves the electrocatalytic activity of bacteria by enhancing cell adhesion, mass transfer of nutrients, and thus thicker biofilm formation. At cathode, high SAV ratio of CNT–based composites paves the way for oxygen adsorption and charge transfer; thus, improves ORR kinetics.

Most of the techniques discussed in this review article are concerned with the electrode modification of MFCs. The CNT composite membranes may also replace conventional membranes like Nafion which not only increase the cost of the device, but also enhances the internal resistance and ohmic losses. There have been numerous advancements in nano–porous membranes with chemical selectivity based on polymer/CNT or graphene composites (Hinds et al., 2004; Khilari et al., 2013; Leong et al., 2015). In this respect, CNT–based membranes are to be studied for their ionic selectivity and exchange capability, while being evaluated against highly efficient Nafion 117 and anion exchange membranes. While acknowledging the study by Venkatesan et al. (Venkatesan and Dharmalingam, 2013) in which chitosan synthesized with MWCNT was used as the separator in a batch–fed mode MFC, research in this field has yet to be continued. The last step towards fast and facile modification of CNT–based MFCs is the electrode preparation methods that are integral parts of MFC manufacturing for commercial levels. Fortunately, fabrication techniques of CNT–based materials are rapidly advancing in various fields of battery industry, fuel cells, and electronics. Many of such reported techniques can also be employed for MFC applications.

All in all, concerns still remain about the reduction mechanism at the cathode which is mostly responsible for limiting the power output of the device, and the anode performance upon which the durability of biomass energy harvesting depends. We expect that research for more biocompatible and efficient microbial anode could also contribute to major improvements in biological hybrid fuel cells (Higgins et al., 2011; Szczupak et al., 2012), and alternative cathodes alleviate the ongoing difficulty of slow ORR kinetics. Hopefully, the rapid development pace in nanoengineered material for energy storage (Huang et al., 2015b; Huang et al., 2016; Vatamanu and Bedrov, 2015) will continue to serve in all aspects the field of MFC.

Appendix A. Supplementary material

Supplementary data associated with this article can be found in the online version at http://dx.doi.org/10.1016/j.bios.2016.05.033.

References

Abdelhalim, A., Abdellah, A., Scarpa, G., Lugli, P., 2013. Carbon 61, 72–79.
Ahn, S.W., Lee, S.S., Lee, S.J., Kim, J.M., 2015. Chem. Eng. Sci. 126, 237–243.
Al Faraj, A., Shaik, A.P., Shaik, A.S., 2015. Int. J. Nanomed. 10, 157.
Amade, R., Vila-Costa, M., Hussain, S., Casamayor, E.O., Bertran, E., 2015. J. Mater. Sci. 50 (3), 1214–1220.
Amirouche, F., Zhou, Y., Johnson, T., 2009. Microsyst. Technol. 15 (5), 647–666.
Antolini, E., 2015. Biosens. Bioelectron. 69, 54–70.
Baker, R., 1989. Carbon 27 (3), 315–323.
Baranitharan, E., Khan, M.R., Prasad, D., Teo, W.F.A., Tan, G.Y.A., Jose, R., 2015. Bioprocess Biosyst. Eng. 38 (1), 15–24.

Bautista-Quijano, J.R., Pötschke, P., Brünig, H., Heinrich, G., 2016. Polymer 82, 181–189.
Berber, S., Kwon, Y.-K., Tománek, D., 2000. Phys. Rev. Lett. 84 (20), 4613.
Bonanni, P.S., Schrott, G.D., Robuschi, L., Busalmen, J.P., 2012. Energy Environ. Sci. 5 (3), 6188–6195.
Bordjiba, T., Mohamedi, M., Dao, L.H., 2008. Adv. Mater. 20 (4), 815–819.
Bosi, S., Ballerini, L., Prato, M., 2014. Carbon Nanotubes in Tissue Engineering. Making and Exploiting Fullerenes, Graphene, and Carbon Nanotubes. Springer, New York, pp. 181–204.
Bottacchi, F., Petti, L., Späth, F., Namal, I., Tröster, G., Hertel, T., Anthopoulos, T.D., 2015. Appl. Phys. Lett. 106 (19), 193302.
Bradford, P.D., Bogdanovich, A.E., 2008. J. Compos. Mater. 42 (15), 1533–1545.
Bradford, P.D., Wang, X., Zhao, H., Zhu, Y.T., 2011. Carbon 49 (8), 2834–2841.
Brewer, B.M., Shi, M., Edd, J.F., Webb, D.J., Li, D., 2014. Biomed. Microdevices 16 (2), 311–323.
Byrne, M.T., Gun'ko, Y.K., 2010. Adv. Mater. 22 (15), 1672–1688.
Cai, D., Mataraza, J.M., Qin, Z.-H., Huang, Z., Huang, J., Chiles, T.C., Carnahan, D., Kempa, K., Ren, Z., 2005. Nat. Methods 2 (6), 449–454.
Canavar, P.E., EKŞİN, E., Erdem, A., 2015. Turk. J. Chem. 39 (1), 1–12.
Carmona-Martínez, A.A., Trably, E., Milferstedt, K., Lacroix, R., Etcheverry, L., Bernet, N., 2015. Water Res. 81, 149–156.
Cassell, A.M., Raymakers, J.A., Kong, J., Dai, H., 1999. J. Phys. Chem. B 103 (31), 6484–6492.
Catal, T., Lesnik, K.L., Liu, H., 2015. Bioresour. Technol. 187, 77–83.
Chang-Jian, S.-K., Ho, J.-R., Cheng, J.J., Sung, C.-K., 2006. Nanotechnology 17 (5), 1184.
Chen, Z., Yuan, Y., Zhou, H., Wang, X., Gan, Z., Wang, F., Lu, Y., 2014. Adv. Mater. 26 (2), 339–345.
Cheng, X., Ye, K., Zhang, D., Cheng, K., Li, Y., Wang, B., Wang, G., Cao, D., 2015. J. Solid State Electrochem. 19 (10), 3027–3034.
Choi, S., 2015. Biosens. Bioelectron. 69, 8–25.
Chou, H.-T., Lee, H.-J., Lee, C.-Y., Tai, N.-H., Chang, H.-Y., 2014. Bioresour. Technol. 169, 532–536.
Christy, M., Jang, H., Nahm, K.S., 2015. J. Power Sources 288, 451–460.
Ci, S., Cai, P., Wen, Z., Li, J., 2015. Sci. China Mater. 58 (6), 496–509.
Correa-Duarte, M.A., Wagner, N., Rojas-Chapana, J., Morsczeck, C., Thie, M., Giersig, M., 2004. Nano Lett. 4 (11), 2233–2236.
Cui, H.-F., Du, L., Guo, P.-B., Zhu, B., Luong, J.H., 2015. J. Power Sources 283, 46–53.
Dalcanale, F., Grossenbacher, J., Blugan, G., Gullo, M.R., Brugger, J., Tevaearai, H., Graule, T., Kuebler, J., 2015. J. Eur. Ceram. Soc. 35 (8), 2215–2224.
Dong, X., Chen, J., Ma, Y., Wang, J., Chan-Park, M.B., Liu, X., Wang, L., Huang, W., Chen, P., 2012. Chem. Commun. 48 (86), 10660–10662.
Du, R., Zhao, Q., Zhang, N., Zhang, J., 2015. Small 11 (27), 3263–3289.
Dubal, D.P., Gund, G.S., Lokhande, C.D., Holze, R., 2013. ACS Appl. Mater. Interfaces 5 (7), 2446–2454.
Erbay, C., Pu, X., Choi, W., Choi, M.-J., Ryu, Y., Hou, H., Lin, F., de Figueiredo, P., Yu, C., Han, A., 2015a. J. Power Sources 280, 347–354.
Erbay, C., Yang, G., de Figueiredo, P., Sadr, R., Yu, C., Han, A., 2015b. J. Power Sources 298, 177–183.
Esser, B., Schnorr, J.M., Swager, T.M., 2012. Angew. Chem. Int. Ed. 51 (23), 5752–5756.
Feng, L., Yan, Y., Chen, Y., Wang, L., 2011. Energy Environ. Sci. 4 (5), 1892–1899.
Franklin, A.D., Luisier, M., Han, S.-J., Tulevski, G., Breslin, C.M., Gignac, L., Lundstrom, M.S., Haensch, W., 2012. Nano Lett. 12 (2), 758–762.
Fu, Y., Yu, J., Zhang, Y., Meng, Y., 2014. Appl. Surf. Sci. 317, 84–89.
Gao, C., Guo, Z., Liu, J.-H., Huang, X.-J., 2012. Nanoscale 4 (6), 1948–1963.
Georgakilas, V., Gournis, D., Tzitzios, V., Pasquato, L., Guldi, D.M., Prato, M., 2007. J. Mater. Chem. 17 (26), 2679–2694.
Ghasemi, M., Daud, W.R.W., Hassan, S.H., Jafary, T., Rahimnejad, M., Ahmad, A., Yazdi, M.H., 2015. Int. J. Hydrog. Energy.
Ghasemi, M., Ismail, M., Kamarudin, S.K., Saeedfar, K., Daud, W.R.W., Hassan, S.H., Heng, L.Y., Alam, J., Oh, S.-E., 2013. Appl. Energy 102, 1050–1056.
Gittleson, F.S., Kohn, D.J., Li, X., Taylor, A.D., 2012. ACS Nano 6 (5), 3703–3711.
Gui, X., Li, H., Wang, K., Wei, J., Jia, Y., Li, Z., Fan, L., Cao, A., Zhu, H., Wu, D., 2011. Acta Mater. 59 (12), 4798–4804.
Gui, X., Wei, J., Wang, K., Cao, A., Zhu, H., Jia, Y., Shu, Q., Wu, D., 2010. Adv. Mater. 22 (5), 617–621.
Halakoo, E., Khademi, A., Ghasemi, M., Yusof, N.M., Gohari, R.J., Ismail, A.F., 2015. Procedia CIRP 26, 473–476.
He, Y.-R., Du, F., Huang, Y.-X., Dai, L.-M., Li, W.-W., H.-Q., Yu, 2016. J. Mater. Chem. A.
Held, M., Schießl, S.P., Miehler, D., Gannott, F., Zaumseil, J., 2015. Appl. Phys. Lett. 107 (8), 083301.
Hernández-Fernández, F., de los Ríos, A.P., Salar-García, M., Ortiz-Martínez, V., Lozano-Blanco, L., Godínez, C., Tomás-Alonso, F., Quesada-Medina, J., 2015. Fuel Process. Technol. 138, 284–297.
Higgins, S.R., Lau, C., Atanassov, P., Minteer, S.D., Cooney, M.J., 2011. ACS Catal. 1 (9), 994–997.
Hinds, B.J., Chopra, N., Rantell, T., Andrews, R., Gavalas, V., Bachas, L.G., 2004. Science 303 (5654), 62–65.
Hoenlein, W., Kreupl, F., Duesberg, G.S., Graham, A.P., Liebau, M., Seidel, R.V., Unger, E., 2004. IEEE Trans. Compon. Packag. Technol. 27 (4), 629–634.
Hopley, E.L., Salmasi, S., Kalaskar, D.M., Seifalian, A.M., 2014. Biotechnol. Adv. 32 (5), 1000–1014.
Huang, J., Zhu, N., Yang, T., Zhang, T., Wu, P., Dang, Z., 2015a. Biosens. Bioelectron. 72, 332–339.
Huang, Y., Hu, H., Huang, Y., Zhu, M., Meng, W., Liu, C., Pei, Z., Hao, C., Wang, Z., Zhi, C., 2015b. ACS Nano 9 (5), 4766–4775.
Huang, Y., Zhu, M., Pei, Z., Xue, Q., Huang, Y., Zhi, C., 2016. J. Mater. Chem. A 4 (4), 1290–1297.
Hyder, M.N., Lee, S.W., Cebeci, F.Ç., Schmidt, D.J., Shao-Horn, Y., Hammond, P.T., 2011. ACS Nano 5 (11), 8552–8561.
Iijima, S., 1991. Nature 354 (6348), 56–58.
Jayasinghe, N., Franks, A., Nevin, K.P., Mahadevan, R., 2014. Biotechnol. J. 9 (10), 1350–1361.
Jiang, Y., Liang, P., Zhang, C., Bian, Y., Yang, X., Huang, X., Girguis, P.R., 2015. Bioresour. Technol. 190, 367–372.
Journet, C., Bernier, P., 1998. Appl. Phys. A Mater. Sci. Process. 67 (1), 1–9.
Journet, C., Maser, W., Bernier, P., Loiseau, A., de La Chapelle, M.L., Lefrant, dlS., Deniard, P., Lee, R., Fischer, J., 1997. Nature 388 (6644), 756–758.
Jung, S.M., Jung, H.Y., Dresselhaus, M.S., Jung, Y.J., Kong, J., 2012. Sci. Rep., 2.
Kabiri, S., Tran, D.N., Altalhi, T., Losic, D., 2014. Carbon 80, 523–533.
Kam, N.W.S., O'Connell, M., Wisdom, J.A., Dai, H., 2005. Proc. Natl. Acad. Sci. USA 102 (33), 11600–11605.
Karousis, N., Tagmatarchis, N., Tasis, D., 2010. Chem. Rev. 110 (9), 5366–5397.
Katuri, K.P., Enright, A.-M., O'Flaherty, V., Leech, D., 2012. Bioelectrochemistry 87, 164–171.
Kavoosi, G., Dadfar, S.M.M., Dadfar, S.M.A., Ahmadi, F., Niakosari, M., 2014. Food Sci. Nutr. 2 (1), 65–73.
Khilari, S., Pandit, S., Ghangrekar, M.M., Pradhan, D., Das, D., 2013. Ind. Eng. Chem. Res. 52 (33), 11597–11606.
Kohlmeyer, R.R., Lor, M., Deng, J., Liu, H., Chen, J., 2011. Carbon 49 (7), 2352–2361.
Korth, B., Rosa, L.F., Harnisch, F., Picioreanu, C., 2015. Bioelectrochemistry.
Kruusenberg, I., Matisen, L., Shah, Q., Kannan, A., Tammeveski, K., 2012. Int. J. Hydrog. energy 37 (5), 4406–4412.
Kumar, A., Karig, D., Acharya, R., Neethirajan, S., Mukherjee, P.P., Retterer, S., Doktycz, M.J., 2013. Microfluid. Nanofluidics 14 (5), 895–902.
Kumar, R., Singh, L., Wahid, Z.A., Din, M.F.M., 2015. Int. J. Energy Res.
Kuntke, P., Sleutels, T., Saakes, M., Buisman, C., 2014. Int. J. Hydrog. Energy 39 (10), 4771–4778.
Kurkina, T., Vlandas, A., Ahmad, A., Kern, K., Balasubramanian, K., 2011. Angew. Chem. Int. Ed. 50 (16), 3710–3714.
Lee, J.H., Lee, J.-Y., Yang, S.H., Lee, E.-J., Kim, H.-W., 2014. Acta Biomater. 10 (10), 4425–4436.
Lee, S.W., Kim, B.-S., Chen, S., Shao-Horn, Y., Hammond, P.T., 2008. J. Am. Chem. Soc. 131 (2), 671–679.
Lee, S.W., Yabuuchi, N., Gallant, B.M., Chen, S., Kim, B.-S., Hammond, P.T., Shao-Horn, Y., 2010. Nat. Nanotechnol. 5 (7), 531–537.
Leong, J.X., Daud, W.R.W., Ghasemi, M., Ahmad, A., Ismail, M., Liew, K.B., 2015. Int. J. Hydrog. Energy 40 (35), 11604–11614.
Li, H., Gui, X., Zhang, L., Wang, S., Ji, C., Wei, J., Wang, K., Zhu, H., Wu, D., Cao, A., 2010. Chem. Commun. 46 (42), 7966–7968.
Li, P., Lei, N., Sheadel, D.A., Xu, J., Xue, W., 2012. Sens. Actuators B: Chem. 166–167, 870–877.
Li, P., Yang, Y., Shi, E., Shen, Q., Shang, Y., Wu, S., Wei, J., Wang, K., Zhu, H., Yuan, Q., 2014. ACS Appl. Mater. Interfaces 6 (7), 5228–5234.
Li, Y., 2016. Sci. China Mater. 59 (2), 93–94.
Li, Z., Zhang, Y., LeDuc, P.R., Gregory, K.B., 2011. Biotechnol. Bioeng. 108 (9), 2061–2069.
Liew, K.B., Daud, W.R.W., Ghasemi, M., Loh, K.S., Ismail, M., Lim, S.S., Leong, J.X., 2015a. Int. J. Hydrog. Energy 40 (35), 11625–11632.
Liew, K.B., Daud, W.R.W., Ghasemi, M., Loh, K.S., Ismail, M., Lim, S.S., Leong, J.X., 2015b. Int. J. Hydrog. Energy.
Lin, Z.-D., Young, S.-J., Chang, S.-J., 2015. Sens. J. IEEE 15 (12), 7017–7020.
Liu, H., Ramnarayanan, R., Logan, B.E., 2004. Environ. Sci. Technol. 38 (7), 2281–2285.
Liu, X.-W., Huang, Y.-X., Sun, X.-F., Sheng, G.-P., Zhao, F., Wang, S.-G., Yu, H.-Q., 2014. ACS Appl. Mater. Interfaces 6 (11), 8158–8164.
Lobo, Ad.O., Antunes, E., Machado, A., Pacheco-Soares, C., Trava-Airoldi, V., Corat, E., 2008. Mater. Sci. Eng.: C 28 (2), 264–269.
Logan, B.E., 2009. Nat. Rev. Microbiol. 7 (5), 375–381.
Logan, B.E., 2010. Appl. Microbiol. Biotechnol. 85 (6), 1665–1671.
Logan, B.E., Call, D., Cheng, S., Hamelers, H.V., Sleutels, T.H., Jeremiasse, A.W., Rozendal, R.A., 2008. Environ. Sci. Technol. 42 (23), 8630–8640.
Logan, B.E., Wallack, M.J., Kim, K.-Y., He, W., Feng, Y., Saikaly, P.E., 2015. Environ. Sci. Technol. Lett. 2 (8), 206–214.
Lou, X., Detrembleur, C., Pagnoulle, C., Jérôme, R., Bocharova, V., Kiriy, A., Stamm, M., 2004. Adv. Mater. 16 (23–24), 2123–2127.
Lu, L., Xing, D., Ren, Z.J., 2015. Bioresour. Technol. 195, 115–121.
Lu, M., Guo, L., Kharkwal, S., Ng, H.Y., Li, S.F.Y., 2013. J. Power Sources 221, 381–386.
Malvankar, N.S., Tuominen, M.T., Lovley, D.R., 2012. Energy Environ. Sci. 5 (2), 5790–5797.
Matsumoto, S., Yamanaka, K., Ogikubo, H., Akasaka, H., Ohtake, N., 2014. Appl. Phys. Lett. 105 (8), 083904.
Mehdinia, A., Ziaei, E., Jabbari, A., 2014. Electrochim. Acta 130, 512–518.
Merrill, M., Sun, C., 2009. Nanotechnology 20 (7), 075606.
Mink, J.E., Hussain, M.M., 2013. ACS Nano 7 (8), 6921–6927.
Mink, J.E., Qaisi, R.M., Logan, B.E., Hussain, M.M., 2014. NPG Asia Mater. 6 (3), e89.
Müller, V., 2016. Science 351 (6268) 34–34.
Mustakeem, M., 2015. Mater. Renew. Sustain. Energy.
Nardecchia, S., Carriazo, D., Ferrer, M.L., Gutiérrez, M.C., del Monte, F., 2013. Chem. Soc. Rev. 42 (2), 794–830.
Nayak, P., Anbarasan, B., Ramaprabhu, S., 2013. J. Phys. Chem. C 117 (25), 13202–13209.

Nguyen, T.-H., Yu, Y.-Y., Wang, X., Wang, J.-Y., Song, H., 2013. Chem. Commun. 49 (91), 10754–10756.
Ormsby, R., McNally, T., O'Hare, P., Burke, G., Mitchell, C., Dunne, N., 2012. Acta Biomater. 8 (3), 1201–1212.
Paloniemi, H., Lukkarinen, M., Ääritalo, T., Areva, S., Leiro, J., Heinonen, M., Haapakka, K., Lukkari, J., 2006. Langmuir 22 (1), 74–83.
Qu, L., Liu, Y., Baek, J.-B., Dai, L., 2010. ACS Nano 4, 1321–1326.
Rao, C.V., Cabrera, C.R., Ishikawa, Y., 2010. J. Phys. Chem. Lett. 1 (18), 2622–2627.
Rao, L., Cai, B., Wang, J., Meng, Q., Ma, C., He, Z., Xu, J., Huang, Q., Li, S., Cen, Y., 2015. Sens. Actuators B: Chem. 210, 328–335.
Rasmussen, M., Minteer, S.D., 2015. Bioelectrochemistry.
Ren, H., Pyo, S., Lee, J.-I., Park, T.-J., Gittleson, F.S., Leung, F.C., Kim, J., Taylor, A.D., Lee, H.-S., Chae, J., 2015. J. Power Sources 273, 823–830.
Ren, H., Torres, C.I., Parameswaran, P., Rittmann, B.E., Chae, J., 2014. Biosens. Bioelectron. 61, 587–592.
Renslow, R., Babauta, J., Kuprat, A., Schenk, J., Ivory, C., Fredrickson, J., Beyenal, H., 2013. Phys. Chem. Chem. Phys. 15 (44), 19262–19283.
Riggs, J.E., Guo, Z., Carroll, D.L., Sun, Y.-P., 2000. J. Am. Chem. Soc. 122 (24), 5879–5880.
Rivera, C.M., Kwon, H.-J., Hashmi, A., Yu, G., Zhao, J., Gao, J., Xu, J., Xue, W., Dimitrov, A.G., 2015. Sensors 15 (5), 10465–10480.
Romeo, T., 2008. Bacterial Biofilms. Springer, Berlin.
Sakimoto, K.K., Wong, A.B., Yang, P., 2016. Science 351 (6268), 74–77.
Shenghua, Z., Nanjian, W., 2007. A novel ultra low power temperature sensor for UHF RFID tag chip. In: Proceedings of the Solid-State Circuits Conference, 2007. ASSCC'07. IEEE Asian, pp. 464–467.
Shi, X., von Dem Bussche, A., Hurt, R.H., Kane, A.B., Gao, H., 2011. Nat. Nanotechnol. 6 (11), 714–719.
Shui, J., Wang, M., Du, F., Dai, L., 2015. Sci. Adv. 1 (1), e1400129.
Song, T.-s., Wu, X.-y., Zhou, C.C., 2013. Appl. Biochem. Biotechnol. 170 (5), 1241–1250.
Souza, V., Husmann, S., Neiva, E., Lisboa, F., Lopes, L., Salvatierra, R., Zarbin, A., 2015. Electrochim. Acta.
Speers, A.M., Reguera, G., 2012. Appl. Environ. Microbiol. 78 (2), 437–444.
Spitalsky, Z., Tasis, D., Papagelis, K., Galiotis, C., 2010. Progress. Polym. Sci. 35 (3), 357–401.
Sui, K., Li, Y., Liu, R., Zhang, Y., Zhao, X., Liang, H., Xia, Y., 2012. Carbohydr. Polym. 90 (1), 399–406.
Sunden, E., Moon, J.K., Wong, C., King, W.P., Graham, S., 2006. J. Vac. Sci. Technol. B 24 (4), 1947–1950.
Szczupak, A., Kol-Kalman, D., Alfonta, L., 2012. Chem. Commun. 48 (1), 49–51.
Tee, P.F., Abdullah, M.O., Tan, I.A.W., Rashid, N.K.A., Amin, M.A.M., Nolasco-Hipolito, C., Bujang, K., 2016. Renew. Sustain. Energy Rev. 54, 235–246.
Thess, A., Lee, R., Nikolaev, P., Dai, H., 1996a. Science 273 (5274), 483.
Thess, A., Lee, R., Nikolaev, P., Dai, H., Petit, P., Robert, J., Xu, C., Lee, Y.H., Kim, S.G., Rinzler, A.G., 1996b. Sci.-AAAS-Wkly. Pap. Ed. 273 (5274), 483–487.
Thostenson, E.T., Ren, Z., Chou, T.-W., 2001. Compos. Sci. Technol. 61 (13), 1899–1912.
Tijing, L.D., Park, C.-H., Choi, W.L., Ruelo, M.T.G., Amarjargal, A., Pant, H.R., Im, I.-T., Kim, C.S., 2013. Compos. Part B: Eng. 44 (1), 613–619.
Treacy, M.J., Ebbesen, T., Gibson, J., 1996.
Urbanski, J.P., Thorsen, T., Levitan, J.A., Bazant, M.Z., 2006. Appl. Phys. Lett. 89 (14), 143508.
Vatamanu, J., Bedrov, D., 2015. J. Phys. Chem. Lett. 6 (18), 3594–3609.
Venkatesan, P.N., Dharmalingam, S., 2013. J. Membr. Sci. 435, 92–98.
Vigolo, D., Al-Housseiny, T.T., Shen, Y., Akinlawon, F.O., Al-Housseiny, S.T., Hobson, R.K., Sahu, A., Bedkowski, K.I., DiChristina, T.J., Stone, H.A., 2014. Phys. Chem. Chem. Phys. 16 (24), 12535–12543.
Vinayan, B., Jafri, R.I., Nagar, R., Rajalakshmi, N., Sethupathi, K., Ramaprabhu, S., 2012. Int. J. Hydrog. Energy 37 (1), 412–421.
Vinoth, V., Wu, J.J., Asiri, A.M., Lana-Villarreal, T., Bonete, P., Anandan, S., 2016. Ultrason. Sonochem. 29, 205–212.
Wang, H., Yang, Y., Liang, Y., Zheng, G., Li, Y., Cui, Y., Dai, H., 2012. Energy Environ. Sci. 5 (7), 7931–7935.
Wang, W., Guo, S., Lee, I., Ahmed, K., Zhong, J., Favors, Z., Zaera, F., Ozkan, M., Ozkan, C.S., 2014a. Sci. Rep., 4.
Wang, W., Guo, S., Penchev, M., Ruiz, I., Bozhilov, K.N., Yan, D., Ozkan, M., Ozkan, C. S., 2013a. Nano Energy 2 (2), 294–303.
Wang, Y., Li, B., Cui, D., Xiang, X., Li, W., 2014b. Biosens. Bioelectron. 51, 349–355.
Wang, Z., Zheng, Y., Xiao, Y., Wu, S., Wu, Y., Yang, Z., Zhao, F., 2013b. Bioresour. Technol. 144, 74–79.
Wen, Z., Ci, S., Mao, S., Cui, S., Lu, G., Yu, K., Luo, S., He, Z., Chen, J., 2013. J. Power Sources 234, 100–106.
Wong, W., Daud, W.R.W., Mohamad, A.B., Kadhum, A.A.H., Loh, K.S., Majlan, E., 2013. Int. J. Hydrog. Energy 38 (22), 9370–9386.
Worsley, M.A., Kucheyev, S.O., Kuntz, J.D., Olson, T.Y., Han, T.Y.-J., Hamza, A.V., Satcher Jr, J.H., Baumann, T.F., 2011. Chem. Mater. 23 (12), 3054–3061.
Wu, W., Zhang, S., Li, Y., Li, J., Liu, L., Qin, Y., Guo, Z.-X., Dai, L., Ye, C., Zhu, D., 2003. Macromolecules 36 (17), 6286–6288.
Wu, Y., Zhang, X., Li, S., Lv, X., Cheng, Y., Wang, X., 2013. Electrochim. Acta 109, 328–332.
Xia, X., Tokash, J.C., Zhang, F., Liang, P., Huang, X., Logan, B.E., 2013. Environ. Sci. Technol. 47 (4), 2085–2091.
Xiao, M., Zhu, J., Feng, L., Liu, C., Xing, W., 2015. Adv. Mater. 27 (15), 2521–2527.
Xu, S., Zhang, Y., Jia, L., Mathewson, K.E., Jang, K.-I., Kim, J., Fu, H., Huang, X., Chava, P., Wang, R., 2014. Science 344 (6179), 70–74.
Yang, Z., Yao, Z., Li, G., Fang, G., Nie, H., Liu, Z., Zhou, X., Chen, Xa, Huang, S., 2011. ACS Nano 6 (1), 205–211.
Yazdi, A.A., Sadeghi, A., Saidi, M.H., 2014. Colloids Surf. A: Physicochem. Eng. Asp. 456, 296–306.
Yazdi, A.A., Sadeghi, A., Saidi, M.H., 2015a. Microfluid. Nanofluidics 19 (6), 1297–1308.
Yazdi, A.A., Sadeghi, A., Saidi, M.H., 2015b. J. Colloid Interface Sci. 442, 8–14.
Yeager, E., 1986. J. Mol. Catal. 38 (1), 5–25.
Yu, D., Goh, K., Wang, H., Wei, L., Jiang, W., Zhang, Q., Dai, L., Chen, Y., 2014. Nat. Nanotechnol. 9 (7), 555–562.
Yu, M.-F., Lourie, O., Dyer, M.J., Moloni, K., Kelly, T.F., Ruoff, R.S., 2000. Science 287 (5453), 637–640.
Zeng, Z., Gui, X., Lin, Z., Zhang, L., Jia, Y., Cao, A., Zhu, Y., Xiang, R., Wu, T., Tang, Z., 2013. Adv. Mater. 25 (8), 1185–1191.
Zhang, M., Yan, Y., Gong, K., Mao, L., Guo, Z., Chen, Y., 2004. Langmuir 20 (20), 8781–8785.
Zhang, Q., Huang, J.Q., Qian, W.Z., Zhang, Y.Y., Wei, F., 2013a. Small 9 (8), 1237–1265.
Zhang, W., Sherrell, P., Minett, A.I., Razal, J.M., Chen, J., 2010. Energy Environ. Sci. 3 (9), 1286–1293.
Zhang, Y., Angelidaki, I., 2014. Water Res. 56, 11–25.
Zhang, Y., Sun, J., Hu, Y., Li, S., Xu, Q., 2013b. J. Power Sources 239, 169–174.
Zhao, J., Hashmi, A., Xu, J., Xue, W., 2012. Appl. Phys. Lett. 100 (24), 243109.
Zhao, Y., Wang, S., Guo, Q., Shen, M., Shi, X., 2013. J. Appl. Polym. Sci. 127 (6), 4825–4832.
Zhu, D., Wang, D.-B., Song, T.-s., Guo, T., Ouyang, P., Wei, P., Xie, J., 2015. Biotechnol. Lett. 37 (1), 101–107.
Zhu, G., He, Z., Chen, J., Zhao, J., Feng, X., Ma, Y., Fan, Q., Wang, L., Huang, W., 2014. Nanoscale 6 (2), 1079–1085.